

Organic Thiocarboxylate Electrodes for a Room-Temperature Sodium-Ion Battery Delivering an Ultrahigh Capacity

Hongyang Zhao⁺, Jianwei Wang⁺, Yuheng Zheng, Ju Li, Xiaogang Han, Gang He,^{*} and Yaping Du^{*}

Abstract: Organic room-temperature sodium-ion battery electrodes with carboxylate and carbonyl groups have been widely studied. Herein, for the first time, we report a family of sodium-ion battery electrodes obtained by replacing stepwise the oxygen atoms with sulfur atoms in the carboxylate groups of sodium terephthalate which improves electron delocalization, electrical conductivity and sodium uptake capacity. The versatile strategy based on molecular engineering greatly enhances the specific capacity of organic electrodes with the same carbon scaffold. By introducing two sulfur atoms to a single carboxylate scaffold, the molecular solid reaches a reversible capacity of 466 mAhg^{-1} at a current density of 50 mA g^{-1} . When four sulfur atoms are introduced, the capacity increases to 567 mAhg^{-1} at a current density of 50 mA g^{-1} , which is the highest capacity value reported for organic sodium-ion battery anodes until now.

Organic battery electrodes are alternatives to traditional metal-oxide electrode materials due to their low costs, absence of heavy metals and easily tunable structures.^[1–15] Generally, organic electrodes accommodate redox centers and alkali-metal ions by functional groups such as carboxylate,^[16] carbonyl,^[17] organodisulfide,^[18] thioether^[19] and nitroxyl radicals,^[20] while the aromatic cores donate or accept electrons during the redox process.^[19] Carboxylate groups are usually applied as lithium/sodium anodes which reversibly store/release Li^+/Na^+ ions through a two-electron process.^[21,22] In the case of a lithium-ion anode, far more than two Li^+ ions can be stored in the carboxylate molecule under

deep discharge,^[23,24] which leads to the high capacity of organic lithium anodes. However, for sodium-ion battery cells, there is no evidence of super-sodiation. The sodium ion is larger and less electronegative than the lithium ion.

Even though the organic sodium-ion battery has a lower specific capacity than the lithium-ion battery, the sodium-ion battery is attractive because of the less rigid lattice compared with metal-oxide lattices, which can accommodate the large sodium ions so that the rate capability and cycle stability are advantageous.^[21] As a classic organic sodium-ion battery anode, the sodium salt of terephthalate (PTA-Na, compound **a** in Figure 1) has a capacity of 295 mAhg^{-1} at a current density of 0.1 C (30 mA g^{-1}),^[16,21] which is comparable to the commonly available hard carbon anodes (ca. 280 mAhg^{-1}) with a charge/discharge plateau of 0.3 V in the half-cell configuration.^[25] Up to now, most of the organic sodium-ion electrodes are composed of oxygen-containing functional groups (carboxylate and carbonyl groups).^[21,26,27] The limitation of these functional groups is that they can only store one sodium ion reversibly, which results in a capacity that is strongly limited by the molecular weight of the molecule.^[28] Another critical issue of organic battery electrodes is their poor conductivity, which limits the specific capacity, rate capability and cycle stability.^[29] Commonly used electrode modifications such as a conductive carbon coating are difficult to realize, because most of the organic compounds decompose at high temperatures.^[30] Apparently, increasing the

[*] H. Zhao,^[†] J. Wang,^[†] Y. Zheng, Prof. G. He, Prof. Y. Du
Frontier Institute of Science and
Technology jointly with College of Science
State Key Laboratory for Strength
and Vibration of Mechanical Structures
Xi'an Jiaotong University, Xi'an, Shaanxi 710054 (China)
E-mail: ganghe@mail.xjtu.edu.cn
ypdu2013@mail.xjtu.edu.cn

Prof. J. Li
Department of Nuclear Science and Engineering and
Department of Materials Science and Engineering
MIT, Cambridge, MA 02139 (USA)

Prof. X. Han
School of Electrical Engineering
The Center of Nanomaterials for Renewable Energy
Xi'an Jiaotong University, Xi'an, Shaanxi 710054 (China)

[†] These authors contributed equally to this work.

Supporting information and the ORCID identification number(s) for the author(s) of this article can be found under:
<https://doi.org/10.1002/anie.201708960>.

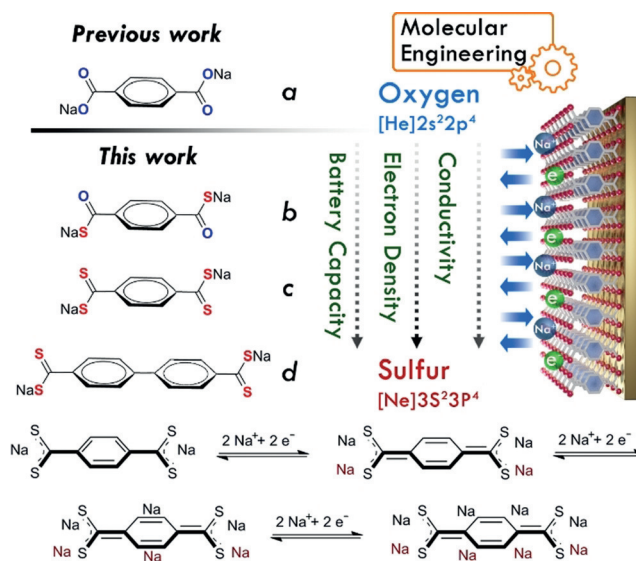


Figure 1. Schematic illustration of sulfur doping into the battery anode.

number of sodium ions stored per carboxylate molecule and improving the intrinsic conductivity of the organic electrodes by chemical modification will significantly enhance the performance of organic batteries.

Recently, organic heteroatom-doped electrode materials have been reported to show obvious advantages, such as many redox centers and a high electric conductivity. For instance, it is reported that nitrogen incorporation into organic molecules enhances the electron density per unit mass.^[31,32] The sulfur atom, which is found in the same group (group VIA) as the oxygen atom, has a larger atomic radius and higher electron density (atomic radius: 100 pm, $[\text{Ne}]3s^23p^4$ for S) relative to the oxygen atom (atomic radius: 60 pm, $[\text{He}]2s^22p^4$ for O). Accordingly, doping sulfur into organic electrodes potentially enhances the conductivity and increases the amount of stored sodium ions. Sodium-ion batteries incorporating these electrode materials possibly show a high specific capacity.^[33]

Based on these considerations and molecular engineering techniques, the O atoms in the PTA-Na molecule (**a**) were replaced by S atoms stepwise to give three sulfur-containing sodium salts (**b**, sodium 1,4-dithiophthalate, **c**, sodium tetrathiophthalate and **d**, sodium 4,4'-biphenyltetrathiodicarboxylate in Figure 1) using a facile one-pot method. First, we successfully incorporated sulfur into the carboxylate groups to form sodium salts of **b**, **c**, and **d** and then we used these molecules for the battery electrodes. The detailed synthesis procedure is listed in the Supporting Information. All target compounds were precipitated at room temperature.

We performed X-ray diffraction (XRD) measurement to study the crystallinity of the synthesized samples. The XRD pattern shows a significant difference in the crystallinity of the samples (see Figures S1 and S2 in the Supporting Information). Scanning electron microscopy (SEM) images show a distinctive difference in the morphology of the four samples. The morphology difference also implies that the crystallinity of molecules **b**, **c** and **d** is not as good as the crystallinity of molecule **a**.

The electric conductivity is one of the most important factors influencing the battery performance. Empirically, white samples are expected to show a poor electric conductivity due to their large bandgap which makes it difficult for the electron to jump from the valence band to the conduction band. As expected, the color of the synthesized samples became darker with increasing sulfur content (Figure S3). The color change indicates not only the incorporation of sulfur atoms, but more importantly, a possibly increasing electric conductivity. As expected, using a four-probe test the measured conductivities of the completely sulfur-substituted samples (**c** and **d**, 4.0 and 1.0 $\mu\text{S cm}^{-1}$, see Figure S5) are much higher than the conductivities measured for the nonsubstituted and partially substituted samples (**a** and **b**, 0.01 and 0.06 $\mu\text{S cm}^{-1}$), which is consistent with DFT calculations. The electrons are more delocalized in the sulfur-containing molecules. The bandgap values reveal the same trend as the conductivity measurements (Table S1).

Four samples were tested as sodium-ion battery anode materials in a coin cell with sodium metal as both counter and reference electrode. Notably, the electrodes barely dissolved in the electrolyte (Figure S4). The redox peaks of the four samples measured against Na/Na^+ were characterized by cyclic voltammetry (CV) (Figure 2a). Interestingly, there are two types of cyclic voltammetry profiles for the molecular solids **a**, **b**, **c** and **d**: for the molecules with oxygen atoms (**a** and **b**), the cyclic voltammograms show a similar profile where the redox peak couple is located at 0–0.5 V. For molecules with solely sulfur atoms (**c** and **d**), the oxidation peaks appears at 2.2 V, and the reduction peaks are located at 0.7 V. The distinct difference between the two types of CV profiles can possibly be derived from the different energy levels of the lowest unoccupied molecular orbital (LUMO). The lower LUMO energy level caused by incorporation of sulfur results in a higher redox potential. Notably, for the molecule with both oxygen and sulfur atoms (molecule **b**), the redox couple appears at 0–0.5 V, but there are also small but

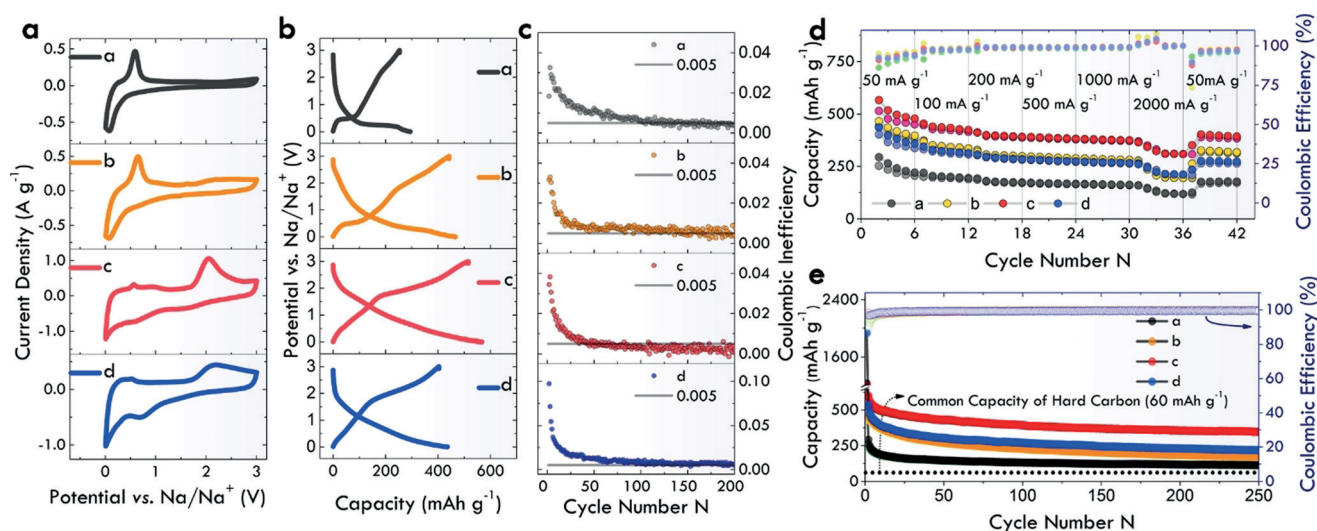


Figure 2. Electrochemical performance of the electrodes. a) Cyclic voltammetry at a scan rate of 0.2 mVs^{-1} . b) Galvanostatic charge–discharge curves. c) Coulombic inefficiency during 200 cycles. d) Rate capability and e) cycle stability at 500 mA g^{-1} .

discernable oxidation and reduction peaks located at 2.2 and 0.7 V, respectively.

Galvanostatic charge–discharge curves for the four compounds show the same trend as revealed by CV measurements. The curves for the molecules with four sulfur atoms (**c** and **d**) show a charge voltage plateau at 2.2 V, and the discharge curve has a slope without a significant discharge plateau. In contrast, the curves for the molecules with one or two oxygen atoms (**a** and **b**) show a significant plateau around 0.5 V. The slope-like discharge plateau for the molecules with four sulfur atoms can possibly be attributed to the low crystallinity after initial discharge.^[24] The charge–discharge curves show that the discharge capacities at a current density of 50 mA g⁻¹ for the four samples are increasing when the number of sulfur atoms increases. Considering the low average voltage plateau and capacity, molecule **b** is a competitive material for the sodium-ion battery. The molecule with one phenyl group and four sulfur atoms (**c**) shows the highest capacity of 567 mAh g⁻¹ which is also the highest capacity of an organic sodium battery electrode reported in literature (Table S4). While the molecule with four sulfur atoms and a biphenyl group (**d**) and the molecules with two sulfur atoms and two oxygen atoms (**b**) have similar capacities (436 and 466 mAh g⁻¹). The molecule containing only oxygen atoms shows the lowest capacity of 294 mAh g⁻¹. The results indicate that replacing sulfur atoms with oxygen atoms can significantly improve the capacity of the electrode. The rate performances of the four molecules are shown in Figure 2 d. The capacity of sulfur-substituted electrodes shows much higher values relative to the PTA-Na molecule at each current density. The excellent rate performance of the molecules suggested that the sulfur-substituted electrode materials maintain a high capacity at a high current rate, which is a reliable method for designing organic electrode materials with a high current rate.

The sulfur-substituted molecules were more stable than pure PTA (**a**). The capacity retention at 500 mA g⁻¹ after 200 cycles is 40%, 40%, 60%, and 43% for **a**, **b**, **c**, and **d**, respectively (Figure 2 e). The initial irreversible capacity retention of molecules **a**, **b**, **c** and **d** is 82%, 66%, 66% and 83%, respectively (Figure S32). The “Coulombic inefficiency” (CI) was plotted for four molecules. For molecule **c**, the CI value decreased below 0.005 after 50 cycles, indicating that the molecule has a highly efficient charge–discharge behavior (Coulombic efficiency > 99.5%) when used as the sodium-ion battery anode. Due to the outstanding performance, molecule **c** was selected as model for the next analyses. The dQ/dV study of molecule **c** showed that during 200 cycles, the charge plateau remained unchanged, implying the redox reaction is highly reversible.^[34]

In order to investigate the charge storage mechanism of the organic anodes, a series of cyclic voltammetry scans was taken from 0.2 to 5 mV s⁻¹ to investigate the portion of the capacitive contribution and the diffusion-controlled contribution.^[35] The total current *I* is defined as the sum of diffusion-controlled current *I_d* and capacitive current *I_c*: $I = I_d + I_c$, where *I_d* is proportional to the square root of the scan rate and *I_c* is proportional to the scan rate. Figure S28 a and b shows the *I_d* and *I_c* for molecule **a** and **c**. The portion of

diffusion-controlled capacity is similar (83% and 84%). Though for the molecule **c**, in the 0–1.5 V region the curves are rectangular-like, diffusion still controls the electrochemical process, indicating a battery-type process is taking place at the full range of electrochemical process.

Raman spectroscopy was used to investigate the structural change of the molecule during the charge–discharge process.^[36] In situ Raman spectroscopy of molecule **c** was performed during the first discharge cycle. The featured peaks of phenyl around 1600 cm⁻¹ and C=S around 1200 cm⁻¹ diminished with increasing discharge depth, indicating that the conjugated organic structure was changed (Figure 3 a). Electrochemical impedance spectroscopy (EIS) measurement can be used to study the kinetics under slight perturbation in the electrochemical cell.^[37] The results show that the contact resistance *R_s* and charge-transfer resistance *R_{ct}* of the sulfur-substituted molecule **c** is smaller than that of pure PTA-Na, which is consistent with the conductivity measurements (Figure 3 c and Figures S5, S30). These results further implied that the capacity and cyclic stability can be enhanced when oxygen is replaced by sulfur as the conductivity increases. As a proof of concept, we also fabricated a flexible cell to demonstrate its potential application in flexible bioelectronics (Figure 3 d and Figure S33).

The sulfur-substituted molecules generally show a better electrochemical performance. The higher electric conductivity makes possible faster electron transport that can compensate the charge imbalance caused by the redox reaction. More importantly, DFT calculation offers an important implication

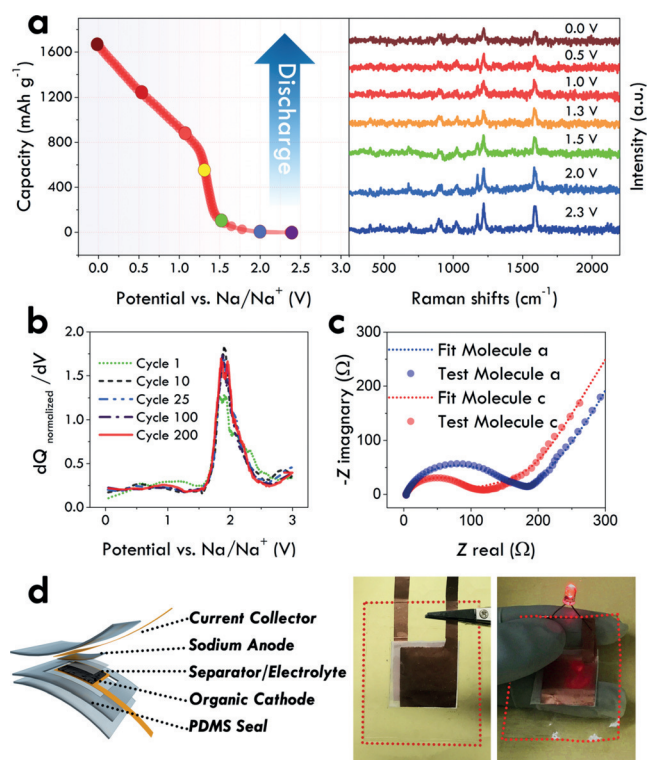


Figure 3. a) In situ Raman spectroscopy for the first discharge cycle. b) dQ/dV of 1st, 10th, 25th, 100th, and 200th cycle. c) EIS analysis of molecule **a** and molecule **c**. d) Prototype of a flexible organic battery.

that the electron-rich sulfur-substituted molecules have the capability to reversibly store additional sodium ions during discharge.^[38] As calculated by DFT (Figure 4 and Fig-

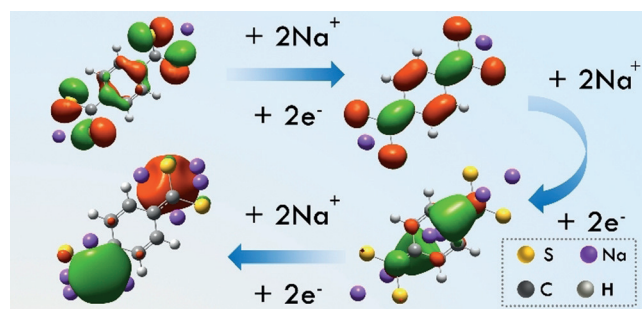


Figure 4. Calculated HOMO plots of molecule **c** with different uptake amounts of sodium.

ure S34,35) molecule **c** can take up maximum six additional sodium ions. The HOMO of molecule **c** with four, six, and eight sodium ions, well-localized within the scaffold, indicates a sufficient stability of **c** and explains the successful supersodiation process,^[38] which is similar to super-lithiation in organic lithium battery electrodes.^[23] Correspondingly, the theoretical capacities of the organic molecules are 255, 443, 586, and 459 mAhg⁻¹ (Table S3). Interestingly, as implied by DFT calculations, the entire sulfur-substituted molecule becomes a sodium reservoir, which is different from PTA-Na, where the sodium ions are only stored at the carboxylate groups. The sodium ions are stabilized on both side of the benzene ring when the molecule takes up six or eight sodium ions. The additional sodium ions can be stored in molecule **c** instead of molecule **a** because the electron density is much higher for sulfur-substituted molecules. A ¹H NMR study was used to get detailed information on the structural changes of the molecules. Compound **a** exhibits before discharge a single strong signal with a chemical shift of $\delta = 7.9$ ppm. After discharging to 0 V, the aromatic proton reversibly shifts and splits into two peaks ($\delta = 6.5$ and 6.7 ppm) (Figure S31). These results not only prove the existence of aromatic structures, but also reflects the destruction of the symmetry of the aromatic system after the discharge process, which is consistent with calculation.

In conclusion, we have developed a family of thiocarboxylate compounds for organic battery electrodes delivering a high capacity. The novel sulfur-substituted compounds can significantly enhance the capacity and cyclic stability compared with the traditional organic electrode based on carboxylic acid. The capacity of the sulfur-substituted molecule is as high as 567 mAhg⁻¹ at a current density of 50 mA g⁻¹ showing high stability and rate performance. The increased capacity after replacing oxygen by sulfur was mainly derived from the decreased bandgap and thus the greatly enhanced electric conductivity and the enhanced sodium-ion uptake of the aromatic rings due to their high electron density. The versatile and efficient strategy offers new chances for developing next-generation high-capacity sodium-ion battery electrodes.

Acknowledgements

We gratefully acknowledge the support from National Key R&D Program of China (2017YFA0208000), the National Natural Science Foundation of China (21371140, 21704081), the China National Funds for Excellent Young Scientists (21522106) and “National Young-1000-Plan” program.

Conflict of interest

The authors declare no conflict of interest.

Keywords: electrochemistry · electrode materials · energy-storage materials · organic batteries · sulfur

How to cite: *Angew. Chem. Int. Ed.* **2017**, *56*, 15334–15338
Angew. Chem. **2017**, *129*, 15536–15540

- [1] Z. Song, Y. Qian, X. Liu, T. Zhang, Y. Zhu, H. Yu, M. Otani, H. Zhou, *Energy Environ. Sci.* **2014**, *7*, 4077.
- [2] Z. Song, Y. Qian, T. Zhang, M. Otani, H. Zhou, *Adv. Sci.* **2015**, *2*, 1500124.
- [3] M. Armand, S. Grugeron, H. Vezin, S. Laruelle, P. Ribiere, P. Poizot, J. M. Tarascon, *Nat. Mater.* **2009**, *8*, 120.
- [4] K. Lei, F. Li, C. Mu, J. Wang, Q. Zhao, C. Chen, J. Chen, *Energy Environ. Sci.* **2017**, *10*, 552.
- [5] S. Yuan, Y. Liu, D. Xu, D. Ma, S. Wang, X. Yang, Z. Cao, X. Zhang, *Adv. Sci.* **2015**, *2*, 1400018.
- [6] Z. Zhu, M. Hong, D. Guo, J. Shi, Z. Tao, J. Chen, *J. Am. Chem. Soc.* **2014**, *136*, 16461.
- [7] T. Sun, Z. Li, H. Wang, D. Bao, F. Meng, X. Zhang, *Angew. Chem. Int. Ed.* **2016**, *55*, 10662; *Angew. Chem.* **2016**, *128*, 10820.
- [8] K. Sakaushi, G. Nickerl, F. M. Wisser, D. Nishio-Hamane, E. Hosono, D. H. Zhou, D. S. Kaskel, D. J. Eckert, *Angew. Chem. Int. Ed.* **2012**, *51*, 7850; *Angew. Chem.* **2012**, *124*, 7972.
- [9] Q. Zhao, J. Wang, Y. Lu, Y. Li, G. Liang, J. Chen, *Angew. Chem. Int. Ed.* **2016**, *55*, 12528; *Angew. Chem.* **2016**, *128*, 12716.
- [10] Z. Song, Y. Qian, M. L. Gordin, D. Tang, T. Xu, M. Otani, H. Zhan, H. Zhou, D. Wang, *Angew. Chem. Int. Ed.* **2015**, *54*, 13947; *Angew. Chem.* **2015**, *127*, 14153.
- [11] A. Abouimrane, W. Weng, H. Eltayeb, Y. Cui, J. Niklas, O. Poluektov, K. Amine, *Energy Environ. Sci.* **2012**, *5*, 9632.
- [12] H. Wang, S. Yuan, D. Ma, X. Zhang, J. Yan, *Energy Environ. Sci.* **2015**, *8*, 1660.
- [13] A. Wild, M. Strumpf, B. Häupler, M. D. Hager, U. S. Schubert, *Adv. Energy Mater.* **2017**, *7*, 1601415.
- [14] S. Yuan, X. Huang, D. Ma, H. Wang, F. Meng, X. Zhang, *Adv. Mater.* **2014**, *26*, 2273.
- [15] X. Huang, D. Xu, S. Yuan, D. Ma, S. Wang, H. Zheng, X. Zhang, *Adv. Mater.* **2014**, *26*, 7264.
- [16] L. Zhao, J. Zhao, Y. S. Hu, H. Li, Z. Zhou, M. Armand, L. Chen, *Adv. Energy Mater.* **2012**, *2*, 962.
- [17] X. Wu, S. Jin, Z. Zhang, L. Jiang, L. Mu, Y. S. Hu, H. Li, X. Chen, M. Armand, L. Chen, X. Huang, *Sci. Adv.* **2015**, *1*, e1500330.
- [18] N. Oyama, T. Tatsuma, T. Sato, T. Sotomura, *Nature* **1995**, *373*, 598.
- [19] L. Zhan, Z. Song, N. Shan, J. Zhang, J. Tang, H. Zhan, Y. Zhou, Z. Li, C. Zhan, *J. Power Sources* **2009**, *193*, 859.
- [20] T. Janoschka, M. D. Hager, U. S. Schubert, *Adv. Mater.* **2012**, *24*, 6397.
- [21] Y. Park, D. S. Shin, S. H. Woo, N. S. Choi, K. H. Shin, S. M. Oh, K. T. Lee, S. Y. Hong, *Adv. Mater.* **2012**, *24*, 3562.

- [22] T. Nokami, T. Matsuo, Y. Inatomi, N. Hojo, T. Tsukagoshi, H. Yoshizawa, A. Shimizu, H. Kuramoto, K. Komae, H. Tsuyama, *J. Am. Chem. Soc.* **2012**, *134*, 19694.
- [23] X. Han, G. Qing, J. Sun, T. Sun, *Angew. Chem. Int. Ed.* **2012**, *51*, 5147; *Angew. Chem.* **2012**, *124*, 5237.
- [24] H. H. Lee, Y. Park, K. H. Shin, K. T. Lee, S. Y. Hong, *ACS Appl. Mater. Interfaces* **2014**, *6*, 19118.
- [25] F. Shen, W. Luo, J. Dai, Y. Yao, M. Zhu, E. Hitz, Y. Tang, Y. Chen, V. L. Sprenkle, X. Li, L. Hu, *Adv. Energy Mater.* **2016**, *6*, 1600377.
- [26] Z. Song, H. Zhan, Y. Zhou, *Angew. Chem. Int. Ed.* **2010**, *49*, 8444; *Angew. Chem.* **2010**, *122*, 8622.
- [27] G. S. Vadehra, R. P. Maloney, M. A. Garcia-Garibay, B. Dunn, *Chem. Mater.* **2014**, *26*, 7151.
- [28] Q. Zhao, Y. Lu, J. Chen, *Adv. Energy Mater.* **2017**, *7*, 1601792.
- [29] H. Wang, S. Yuan, D. Ma, X. Huang, F. Meng, X. Zhang, *Adv. Energy Mater.* **2014**, *4*, 1301651.
- [30] S. Wang, L. Wang, Z. Zhu, Z. Hu, Q. Zhao, J. Chen, *Angew. Chem. Int. Ed.* **2014**, *53*, 5892; *Angew. Chem.* **2014**, *126*, 6002.
- [31] C. Peng, G. H. Ning, J. Su, G. Zhong, W. Tang, B. Tian, C. Su, D. Yu, L. Zu, J. Yang, M. F. Ng, Y. S. Hu, Y. Yang, M. Armand, K. P. Loh, *Nat. Energy* **2017**, *2*, 17074.
- [32] J. Hong, M. Lee, B. Lee, D. H. Seo, C. B. Park, K. Kang, *Nat. Commun.* **2014**, *5*, 5335.
- [33] S. N. Talapaneni, T. H. Hwang, H. J. Sang, O. Buyukcakir, J. W. Choi, A. Coskun, *Angew. Chem. Int. Ed.* **2016**, *55*, 3106; *Angew. Chem.* **2016**, *128*, 3158.
- [34] M. Sathiya, A. M. Abakumov, D. Foix, G. Rousse, K. Ramesha, M. Saubanère, M. Doublet, H. Vezin, C. Laisa, A. Prakash, *Nat. Mater.* **2015**, *14*, 230.
- [35] J. Wang, J. Polleux, J. Lim, B. Dunn, *J. Phys. Chem. C* **2007**, *111*, 14925.
- [36] R. Baddour-Hadjean, J. P. Pereira-Ramos, *Chem. Rev.* **2010**, *110*, 1278.
- [37] J. P. Diard, B. Le Gorrec, C. Montella, *J. Power Sources* **1998**, *70*, 78.
- [38] H. Wang, S. Yuan, Z. Si, X. Zhang, *Energy Environ. Sci.* **2015**, *8*, 3160.

Manuscript received: August 30, 2017

Accepted manuscript online: October 5, 2017

Version of record online: November 2, 2017

Supporting Information

Organic Thiocarboxylate Electrodes for a Room-Temperature Sodium-Ion Battery Delivering an Ultrahigh Capacity

Hongyang Zhao⁺, Jianwei Wang⁺, Yuheng Zheng, Ju Li, Xiaogang Han, Gang He, and Yaping Du**

anie_201708960_sm_miscellaneous_information.pdf

Supporting Information

Table of Contents

S1. Materials and instrumentation	3
S2. Computational methods	3
S3. Detailed experiment	4
S4. SEM images.....	7
S5. XRD patterns	8
S6. Digital photos of four sodium salts.....	9
S7. Electric conductivities of four sodium salts	11
S8. Computational results	12
S9. FT-IR spectra	14
S10. TGA curves	15
S11. Computed and experimental UV-vis excitation spectra	16
S12. Cyclic voltammograms in DMF.....	20
S13. NMR spectra of the sulfur-substituted dicarboxylate	21
S14. Electrochemical results	25
S15. Comparison of the present sodium anode materials	33
S16. Coordinates of molecular structures.....	35
S17. References.....	44
Author Contributions.....	44

S1. Materials and instrumentation

General. p-xylylene dichloride (98%), 4,4'-bis(chloromethyl) biphenyl (98%) and sulfur powder (99.5%) were purchased from Energy Chemical Inc. Dithioterephthalic acid (98%) was obtained from Sigma-Aldrich.

NMR spectra were measured on a Bruker Avance-400 spectrometer in the solvents indicated; chemical shifts are reported in units (ppm) by assigning TMS resonance in the ^1H spectrum as 0.00 ppm, $(\text{CD}_3)_2\text{SO}$ resonance in the ^{13}C spectrum as 39.52 ppm. Coupling constants are reported in Hz with multiplicities denoted as s (singlet), d (doublet), t (triplet), q (quartet) and m (multiplet). FT-IR spectra were measured by a Nicolet 6700 FT-IR spectrometer. UV-vis measurements were performed using DH-2000-BAL Scan spectrophotometer. Cyclic voltammograms (CVs) were performed using a CHI660E electrochemical analyzer. Thermogravimetric analysis (TGA) measurements were carried out in the temperature range of 30-700°C by using of a Mettler-Toledo TGA1 thermal analyzer in air, at a heating rate of 10K min⁻¹. Battery performance was tested on LAND battery testing systems at 40°C. Electrochemical impedance spectroscopy was performed on Autolab PGSTAT302N electrochemical workstation.

S2. Computational methods

All the computational calculations reported in this work were performed using the Gaussian 09 code.^[1]

To implicitly simulate the influence of water and DMF, the Polarizable Continuum Model (PCM)^[2] as a self-consistent reaction field (SCRF) was used for the calculation of equilibrium geometries, vibrational frequencies, excited state calculations. For comparison with experimental UV-Vis, water was used for compound **a** and N, N-dimethylformamide (DMF) was used for compounds **b**, **c**, **d** as implicit solvent.

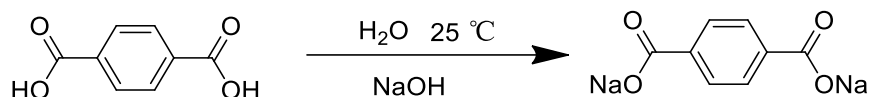
The geometry of compounds **a**, **b**, **c**, **d** in both in the gas phase and in the solutions were optimized and harmonic frequencies calculated at the density functional theory (DFT)^[3,4] level at M06-2X^[5,6] levels with 6-311++G(d,p) basis set.

The simulated UV-Vis spectra and molecular orbitals (MOs) for optimized molecules were performed at the time dependent density functional theory (TD-DFT)^[7,8] at the ground-state equilibrium geometries to both low-lying

singlet and triplet states were determined using the PBE0^[9] framework with 6-311++G(d,p) basis set in two representative solvents using the PCM model:(1) H₂O for **a** and (2) DMF for **b**, **c**, **d**.

S3. Detailed experiment

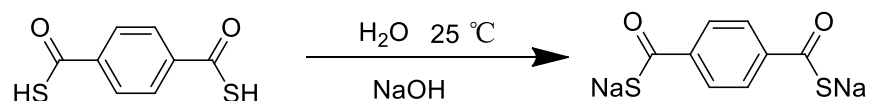
Synthesis of compound **a**



An aqueous solution (5 mL) of NaOH (1.20 g, 0.03 mol) was transferred to a stirred aqueous suspension (20 mL) of terephthalic acid (1.66 g, 0.01 mol) at room temperature. After the completion of the reaction, the solution was filtered and then ethanol (25 mL) was added to the filtrate, resulting in white precipitates. The precipitate was filtered, washed with ethanol to give compound **a** as white solid. Yield: 1.72 g (82%).

¹H NMR (400 MHz, D₂O): δ 7.82 (s, 4H); ¹³C NMR (100 MHz, D₂O): δ 175.30, 138.61, 128.53. UV/vis (in H₂O): λ_{max} (ε) = 240 nm (9.60 × 10³ M⁻¹ cm⁻¹).

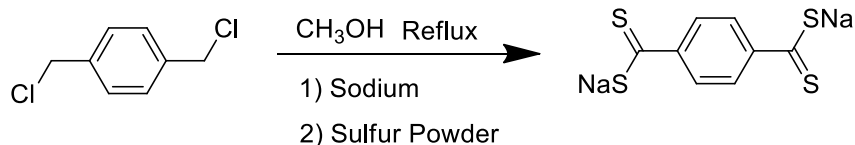
Synthesis of compound **b**



An aqueous solution (2 mL) of NaOH (40 mg, 1 mmol) was transferred to a stirred aqueous suspension (8 mL) of dithioterephthalic acid (198 mg, 1 mmol) at room temperature. After the completion of the reaction, the solution was filtered and then dried by a freezer-dryer to give compound **b** as yellow solid. Yield: 202 mg (83%).

¹H NMR (400 MHz, DMSO-*d*₆): δ 8.03 (s, 4H); ¹³C NMR (100 MHz, DMSO-*d*₆): δ 167.30, 135.01, 130.06. This compound decomposes without melting. UV/vis (in DMF): λ_{max} (ε) = 338 nm (3.69 × 10³ M⁻¹ cm⁻¹).

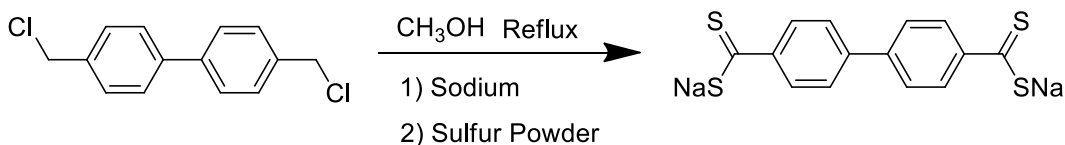
Synthesis of compound **c**



Sodium (0.92 g, 0.04 mol) and sulfur powder (1.28 g, 0.04 mol) was dissolved in dry methanol (100 mL). This mixture was heated to reflux for 4 h under argon in a two-necked flask equipped with a reflux condenser. Then, p-xylylene dichloride (1.75 g, 0.01 mol) was added to the reaction mixture in small portions over a period of 1 h. The reaction was allowed to reflux for additional 15 h, generating a red solution with some solids suspended. After the solution was cooled at room temperature, methanol was removed under reduced pressure. The dark red solid was redissolved in THF (50 mL), and then the solution was filtered. Hexane (20 mL) was added to the filtrate, and cooled to -15°C . The precipitation was collected by filtration to yield compound **c** as dark red solid. Yield: 1.64 g (60%).

^1H NMR (400 MHz, DMSO-d_6): δ 7.89 (s, 4H); ^{13}C NMR (100 MHz, DMSO-d_6): δ 249.94, 152.18, 124.49. This compound decomposes without melting. UV/vis (in THF): $\lambda_{\text{max}}(\epsilon) = 333 \text{ nm}$ ($9.81 \times 10^3 \text{ M}^{-1} \text{ cm}^{-1}$).

Synthesis of compound **d**



Sodium (0.92 g, 0.04 mol) and sulfur powder (1.28 g, 0.04 mol) was dissolved in dry methanol (100 mL). This mixture was heated to reflux for 4 h under argon in a two-necked flask equipped with a reflux condenser. Then, 4,4'-bis(chloromethyl) biphenyl (2.51 g, 0.01 mol) was added to the reaction mixture in small portions over a period of 1 h. The reaction was allowed to reflux for additional 15 h, generating a red solution with some solids suspended. After the solution was cooled at room temperature, methanol was removed under reduced pressure. The dark red solid was redissolved in THF (50 mL), and then the solution was filtered. Hexane (20 mL) was added to the filtrate, and it was cooled to -15°C . The precipitation was collected by filtration to yield compound **d** as dark red solid. Yield: 2.24 g (64%).

^1H NMR (400 MHz, DMSO-d_6): δ 8.23 (d, $J = 8.4 \text{ Hz}$, 4H), 7.47 (d, $J = 8.5 \text{ Hz}$, 4H); ^{13}C NMR (100 MHz, CDCl_3): δ 248.96, 151.36, 139.44, 126.98, 124.27. This compound decomposes without melting. UV/vis (in DMF): $\lambda_{\text{max}}(\epsilon) = 335 \text{ nm}$ ($2.08 \times 10^4 \text{ M}^{-1} \text{ cm}^{-1}$).

Electrochemical measurements**a. Cyclic voltammetry in solution**

Cyclic voltammetry was conducted in a Ar-filled glove box with oxygen and water content lower than 0.1 ppm. Three-electrode configuration was adopted where a gold plate was used as working electrode, a platinum mesh was used as counter electrode, and Ag/AgCl filled with electrolyte was used as reference electrode in 0.10 M Bu_4NPF_6 solution in degassed and dried DMF. The scan rate is 50 mV/s. Potentials are determined against a ferrocene/ferrocenyl ion couple (Fc/Fc^+).

b. Battery assembling

The battery electrodes was prepared by conventional slurry coating method where active material:carbon black:CMC = 6:3:1. 30 mg of mixed powder was grounded and stirred in ~1 mL mixture of water/ethanol overnight to form a viscous slurry. The slurry was then coated on copper foil with a doctor blade. The electrodes were dried in vacuum at 80°C for 6 h and then punched into round disks with diameter of 12 mm. The active material loading on copper current collector was ~1 mg cm^{-2} . The sodium battery was assembled in CR2032 coin cell in an Ar-filled glove box with oxygen and water content lower than 0.1 ppm. Sodium disk with diameter of 12 mm and thickness of 1 mm was used as both counter and reference electrode; a piece of glass fiber (diameter = 16mm) was used as separator, and 60 μL 1 M NaClO_4 in ethylene carbonate(EC)/ dimethyl ethylene carbonate (DMC) (1:1 Vol%) with 5% fluoroethylene carbonate (FEC) was used as electrolyte for each cell. The battery cells were stand for 12 h before test.

S4. SEM images

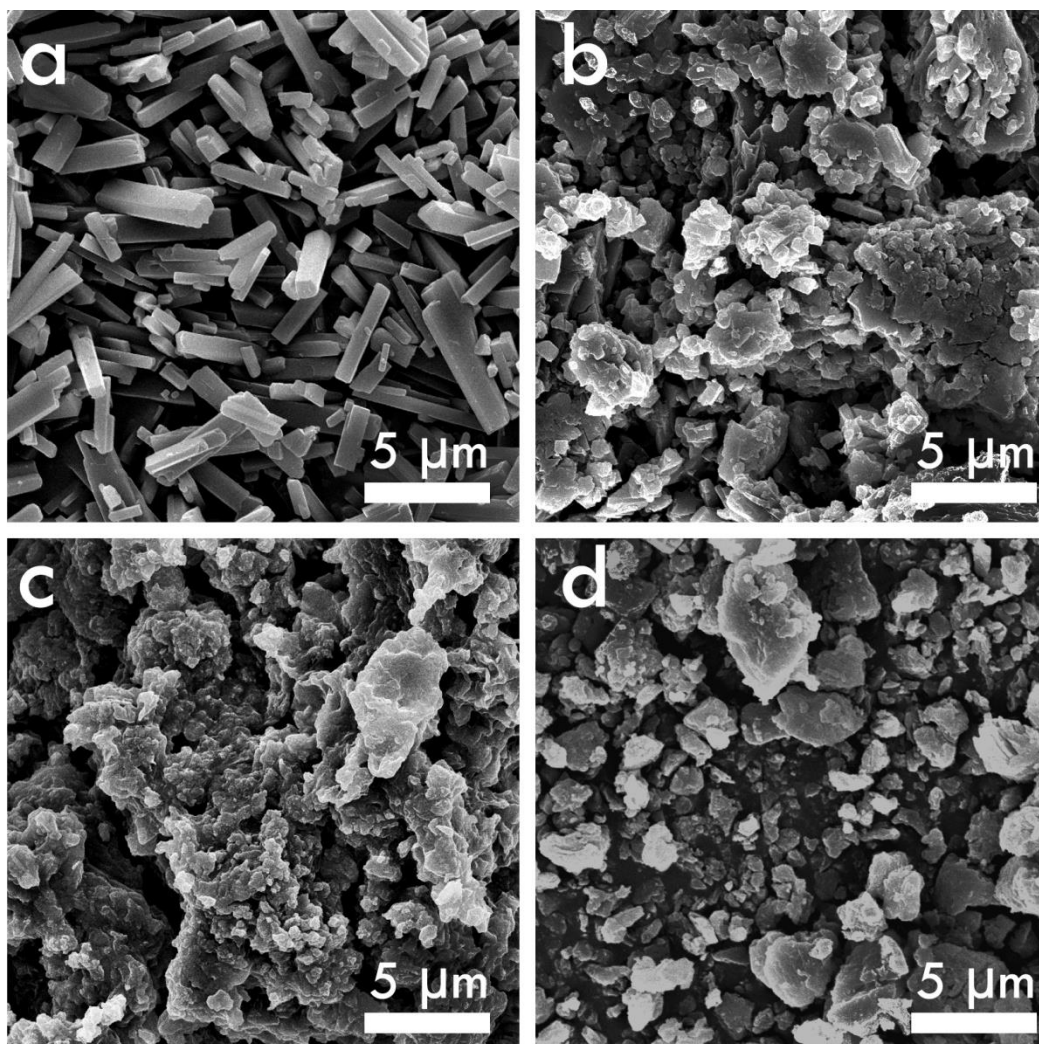


Figure S1. SEM images of sample a, b, c, and d. The scale bars of four images are 10 μm.

S5. XRD patterns

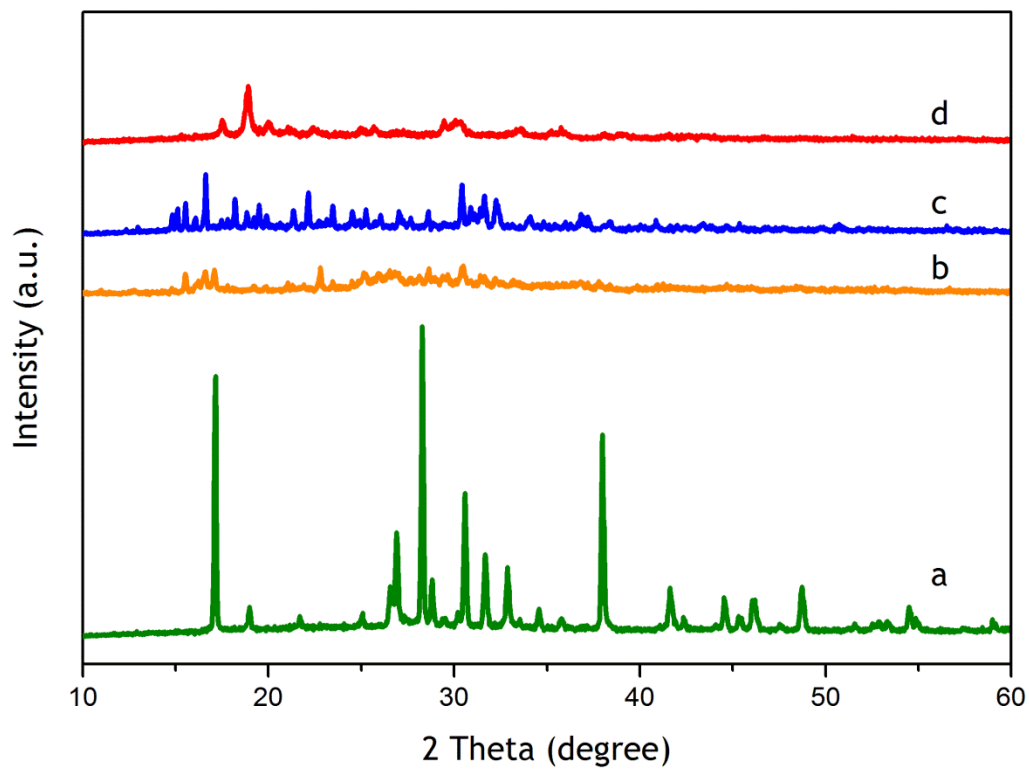


Figure S2. XRD patterns of sample **a**, **b**, **c**, and **d**.

S6. Digital photos of four sodium salts

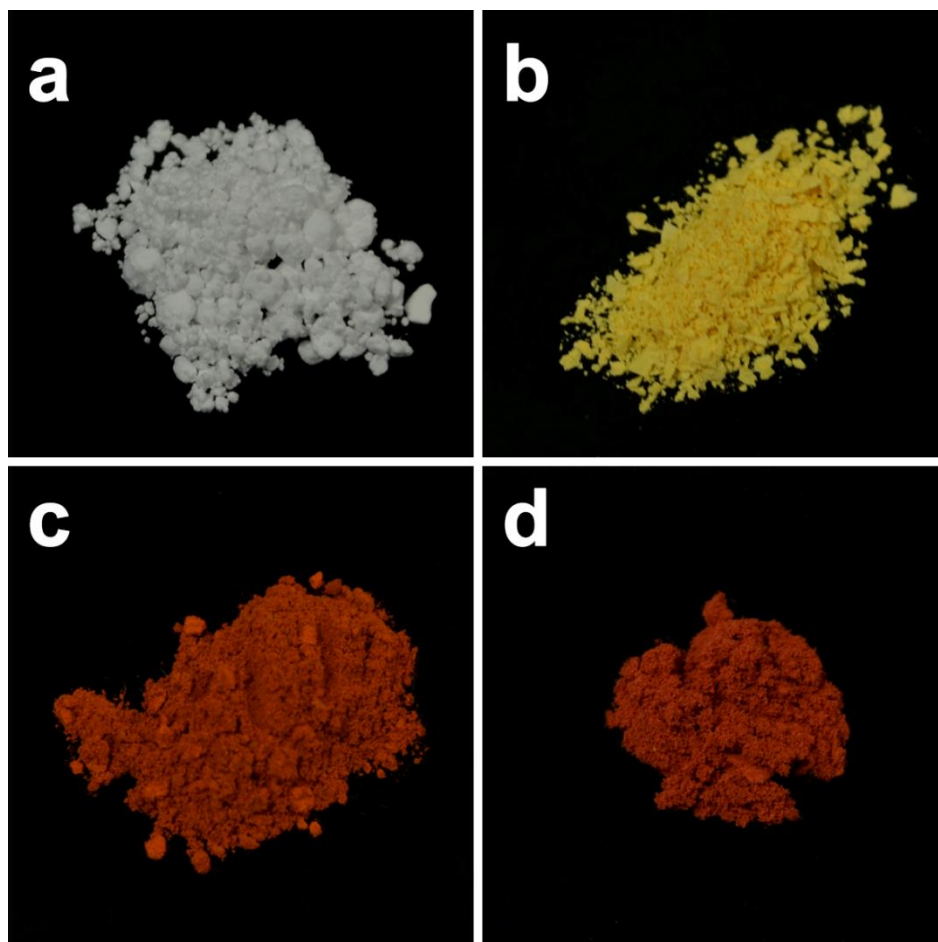


Figure S3. Digital photos of prepared four organic salts. The sodium terephthalate (**a**) exhibits the white color; the sodium 1,4-dithioterephthalate (**b**) exhibits the yellow color; both sodium tetrathioterephthalate (**c**) and sodium 4,4'-Biphenyltetrathiodicarboxylate (**d**) exhibit the dark red color.

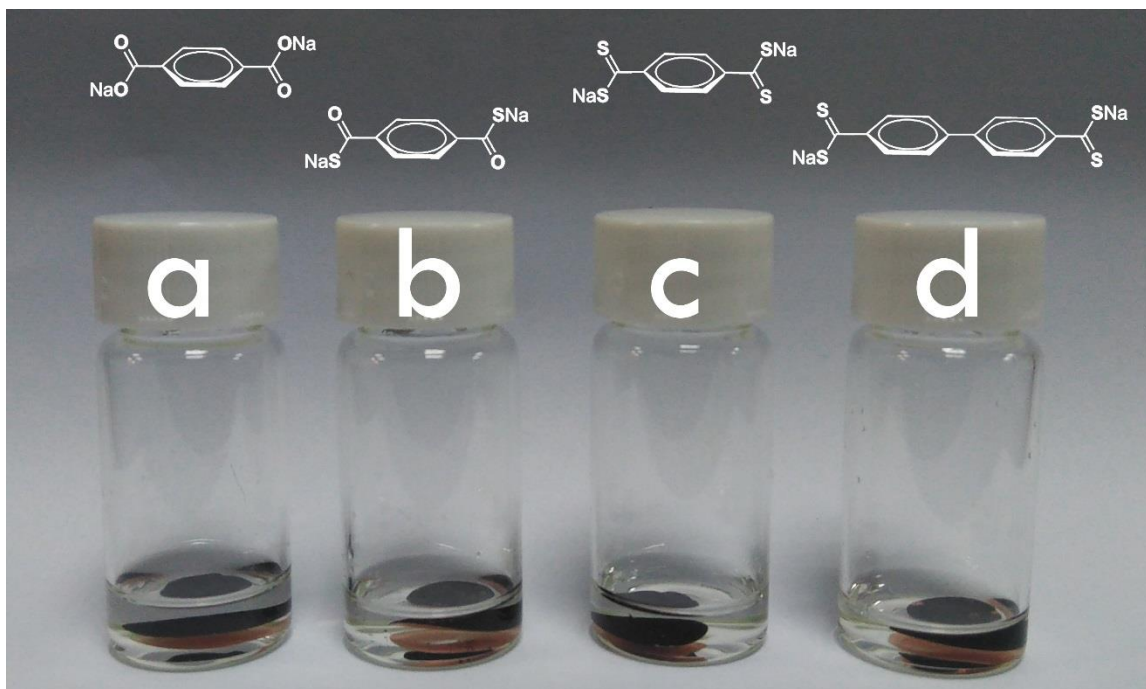


Figure S4. Solubility test of four molecular electrodes **a**, **b**, **c** and **d**

S7. Electric conductivities of four sodium salts

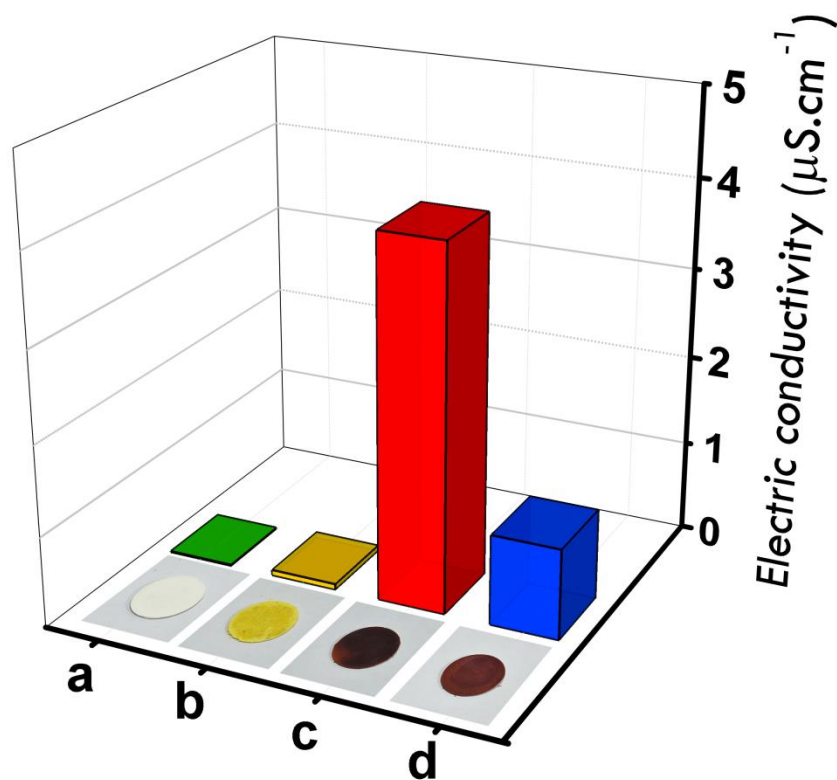


Figure S5. The electric conductivities of four sodium salts.

The electric conductivities of **a** and **b** are about 0.01 and 0.06 $\mu\text{S}\cdot\text{cm}^{-1}$, respectively. As comparison, the electric conductivities of **c** and **d** are about 4 and 1 $\mu\text{S}\cdot\text{cm}^{-1}$, which are higher than the values of **a** and **b**.

S8. Computational results

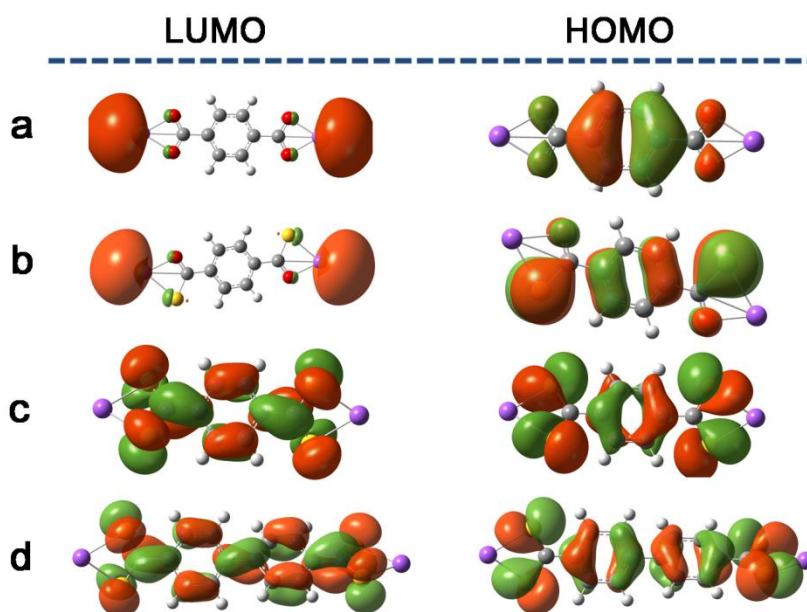
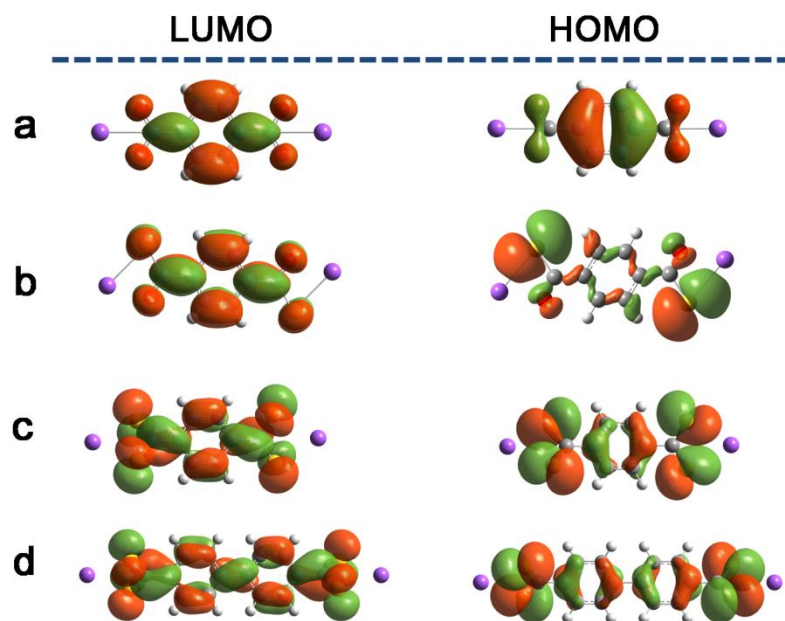


Figure S6. Calculated LUMO and HOMO orbitals for salts in the gas phase.

Figure S7. Calculated LUMO and HOMO orbitals for **a** in H₂O and **b**, **c**, **d** in DMF.

DFT calculations with an isocontour value of 0.03 at the M06-2X/6-311++G(d,p) level of theory were performed to elucidate the electronic structures of the four sodium salts. The optimized geometries in both the gas phase and the liquid phase are shown in Figure S5 and Figure S6, respectively.

Table S1. Electrochemical potentials and energy levels of the organic salts

salts	E_{red} (V) ^a	E_g (eV) ^b	LUMO (eV) ^c	HOMO (eV) ^d	E_g (eV) ^e	E_g (eV) ^g
a	-1.35	4.76	-3.45	-8.21	6.29	7.87
b	-1.09	3.18	-3.71	-6.89	5.78	6.15
c	-0.67	2.80	-4.13	-6.93	5.39	5.27
d	-0.82	2.86	-3.98	-6.84	5.50	5.41

a. Reduction potentials measured by cyclic voltammetry with ferrocene as the standard (the oxidation potential of ferrocene set as zero).

b. Band gap estimated from the UV-vis absorption spectrum.

c. Calculated from the reduction potentials

d. Deduced from the LUMO and E_g . HOMO = LUMO - E_g ^b

e. Band gap is calculated in the gas phase by computational calculation.

g. Band gap is calculated **a** in H₂O and **b, c, d** in DMF by computational calculation.

S9. FT-IR spectra

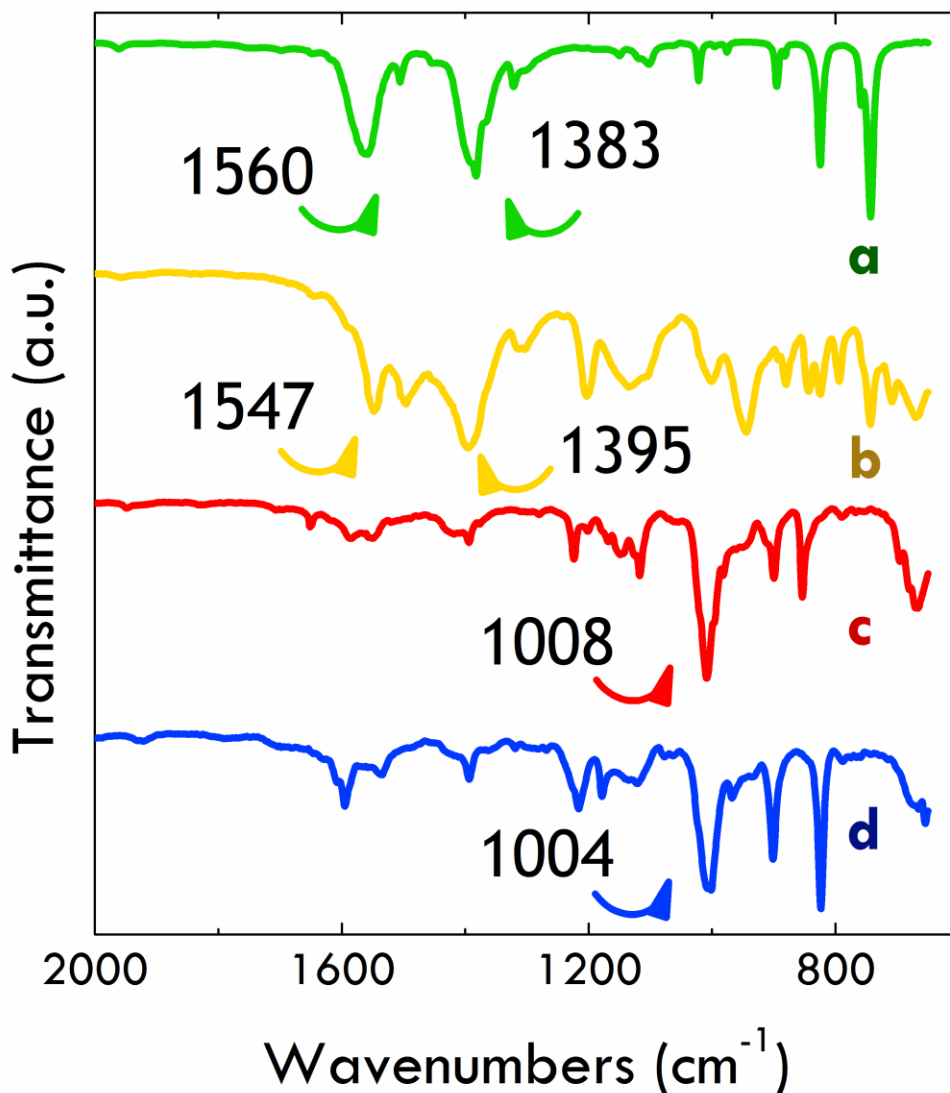


Figure S8. FT-IR spectra of **a**, **b**, **c** and **d**; all the spectra were measured by using attenuated total reflectance (ATR) technique.

The sodium coordination compounds of **a**($\text{Na}_2\text{C}_8\text{H}_4\text{O}_4$), **b**($\text{Na}_2\text{C}_8\text{H}_4\text{O}_2\text{S}_2$), **c**($\text{Na}_2\text{C}_8\text{H}_4\text{S}_4$) and **d**($\text{Na}_2\text{C}_{14}\text{H}_8\text{S}_4$) were further verified by Fourier transform infrared (FT-IR) spectroscopy. As shown in Figure S7, the spectrum of $\text{Na}_2\text{C}_8\text{H}_4\text{O}_4$ showed two typical bands at 1560 and 1383 cm^{-1} , which were assigned to asymmetric and symmetric stretching vibrations, respectively. Interestingly, the two peaks of $\text{Na}_2\text{C}_8\text{H}_4\text{O}_2\text{S}_2$ belonging to the absorption of -COSNa groups obviously shift to wave-number of 1547 and 1395 cm^{-1} in comparison with the $\text{Na}_2\text{C}_8\text{H}_4\text{O}_4$, which

were caused by S substituent. The most important feature observable in the spectra of $\text{Na}_2\text{C}_8\text{H}_4\text{S}_4$ and $\text{Na}_2\text{C}_{14}\text{H}_8\text{S}_4$ is the (CSS⁻) band at 1008 and 1004 cm^{-1} , respectively.

S10. TGA curves

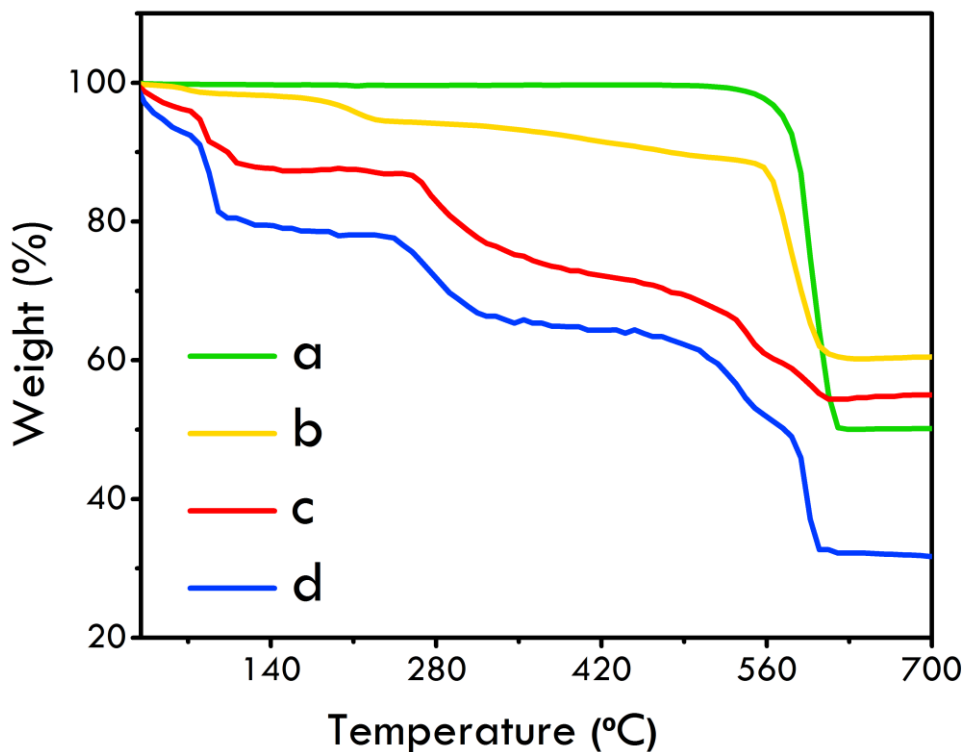


Figure S9. Thermogravimetric analysis of four sodium salts without annealing process.

The samples were heated at a rate of 10 K min^{-1} from room temperature to 700°C in the air. It can be seen from TGA that compound **a** and **b** started to decompose at ~550°C; While the molecule **c** and **d** decomposed at ~240°C. The weight loss for molecule **c** and **d** at 240°C and 550°C might correspond to the loss of sulfur when heated. Though molecule **c** and **d** are less stable than molecule **a** and **b** under high temperature, the sodium ion battery usually operates under room temperature, thus all the molecules are suitable candidates for battery electrodes.

S11. Computed and experimental UV-vis excitation spectra

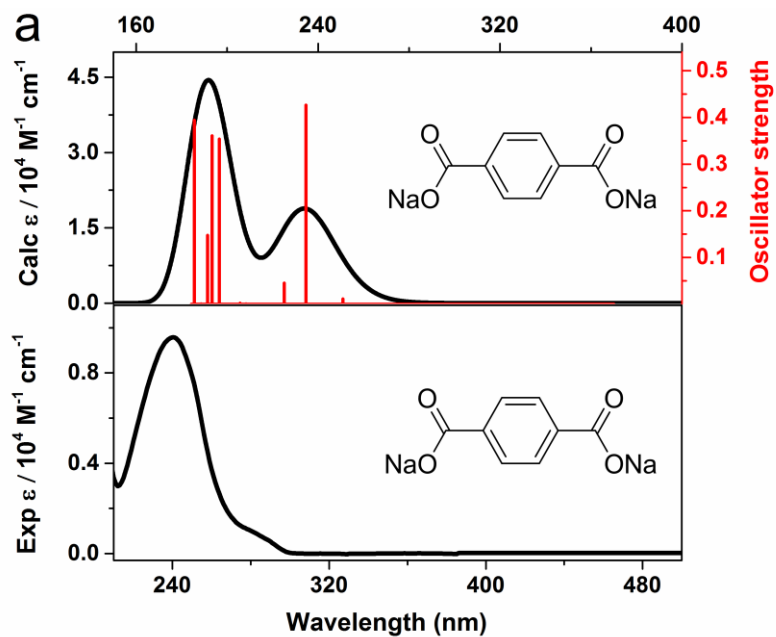


Figure S10. (top) Computed UV-vis spectrums of **a** in water at the TD-PBE0/6-311++G(d,p) level of theory in the PCM model; (down) experimental UV-vis spectra of **a** (3×10^{-5} mol/L) in H₂O.

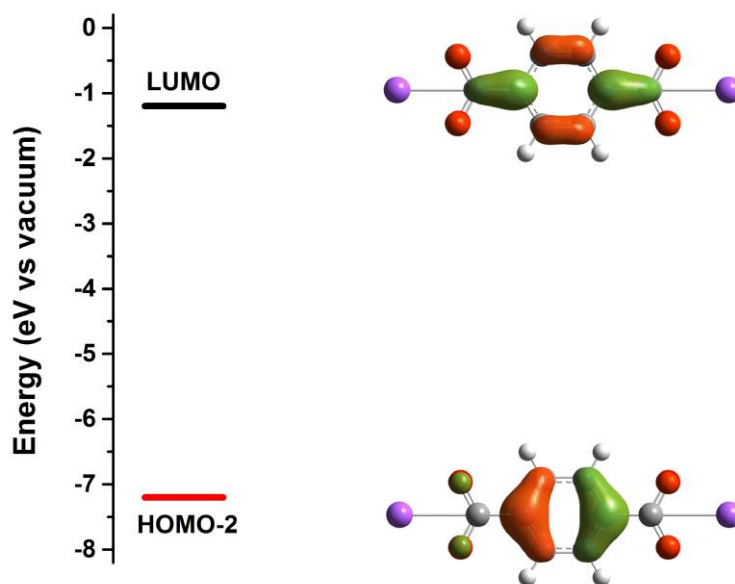


Figure S11. Computed frontier orbitals of **a** in water with an isocontour value of 0.05 at the TD-PBE0/6-311++G(d,p) level of theory in the PCM model.

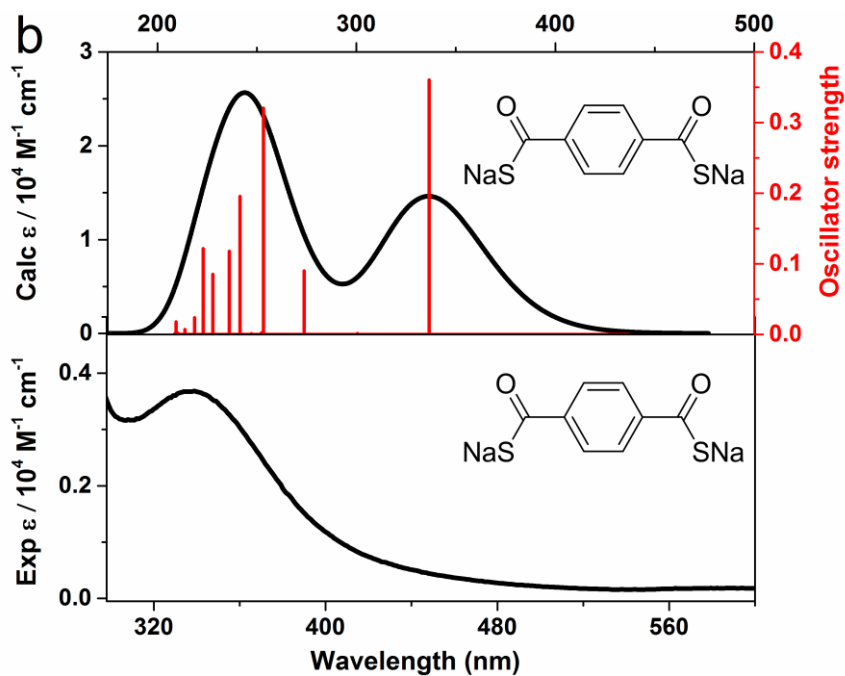


Figure S12. (top) Computed UV-vis spectrums of **b** in DMF at the TD-PBE0/6-311++G(d,p) level of theory in the PCM model; (down) experimental UV-vis spectra of **b** ($3 \times 10^{-5} \text{ mol/L}$) in DMF.

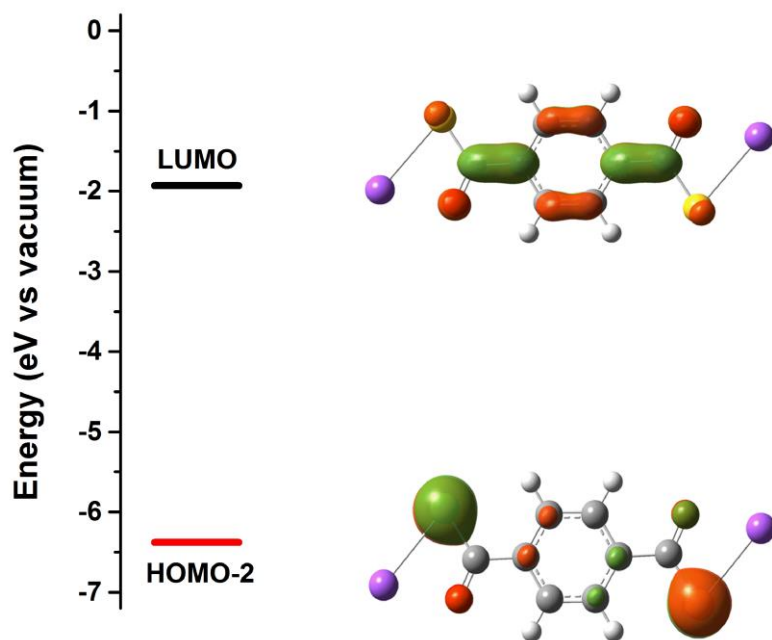


Figure S13. Computed frontier orbitals of **b** in DMF with an isocontour value of 0.05 at the TD-PBE0/6-311++G(d,p) level of theory in the PCM model.

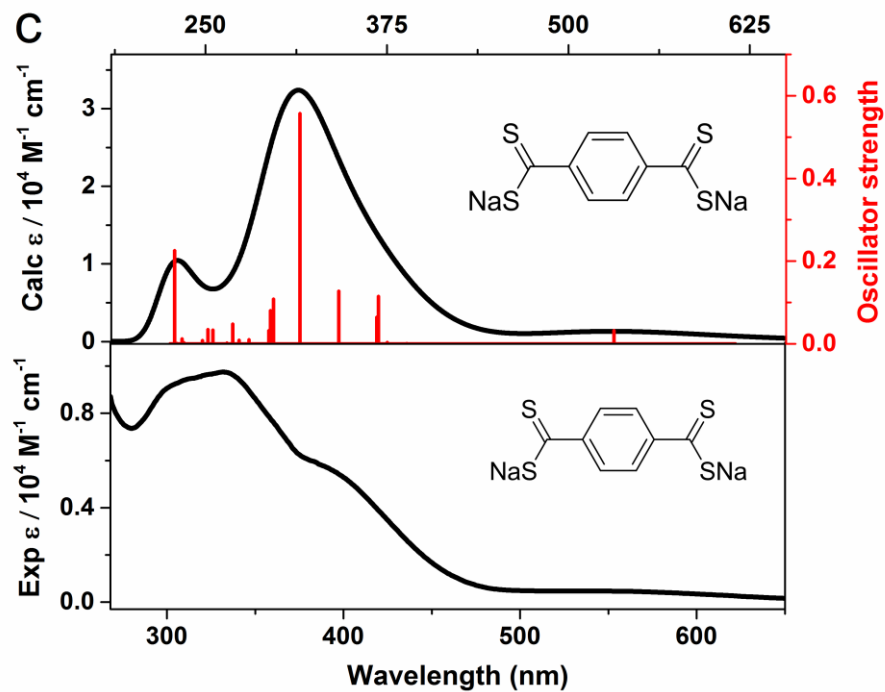


Figure S14. (top) Computed UV-vis spectrums of **c** in DMF at the TD-PBE0/6-311++G(d,p) level of theory in the PCM model; (down) experimental UV-vis spectra of **c** ($3 \times 10^{-5} \text{ mol/L}$) in DMF.

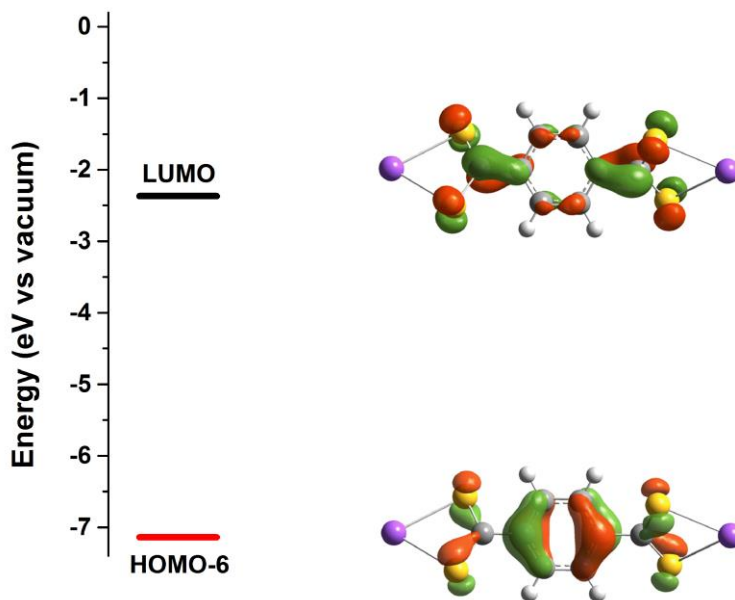


Figure S15. Computed frontier orbitals of **c** in DMF with an isocontour value of 0.05 at the TD-PBE0/6-311++G(d,p) level of theory in the PCM model.

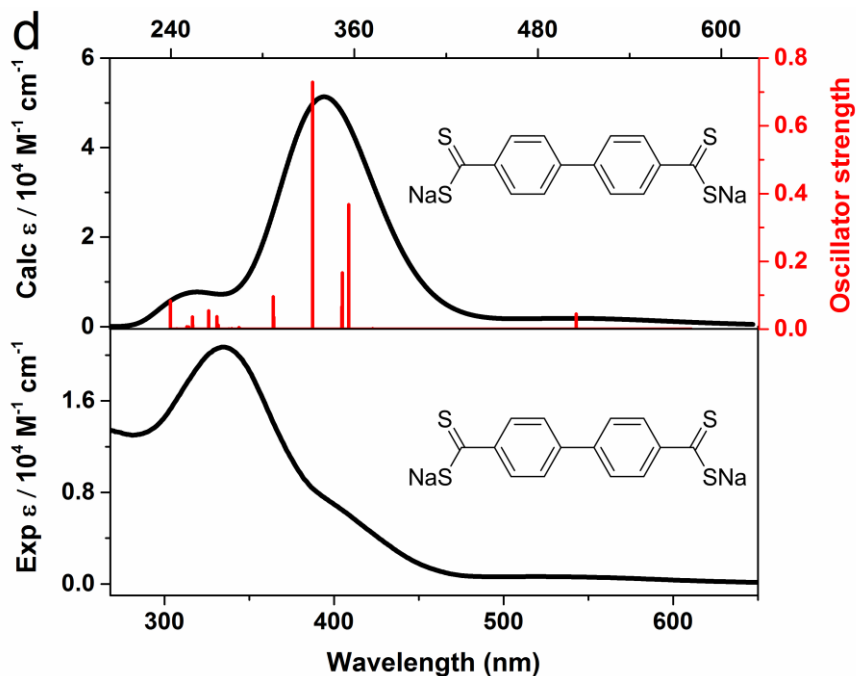


Figure S16. (top) Computed UV-vis spectrums of **d** in DMF at the TD-PBE0/6-311++G(d,p) level of theory in the PCM model; (down) experimental UV-vis spectra of **d** (3×10^{-5} mol/L) in DMF.

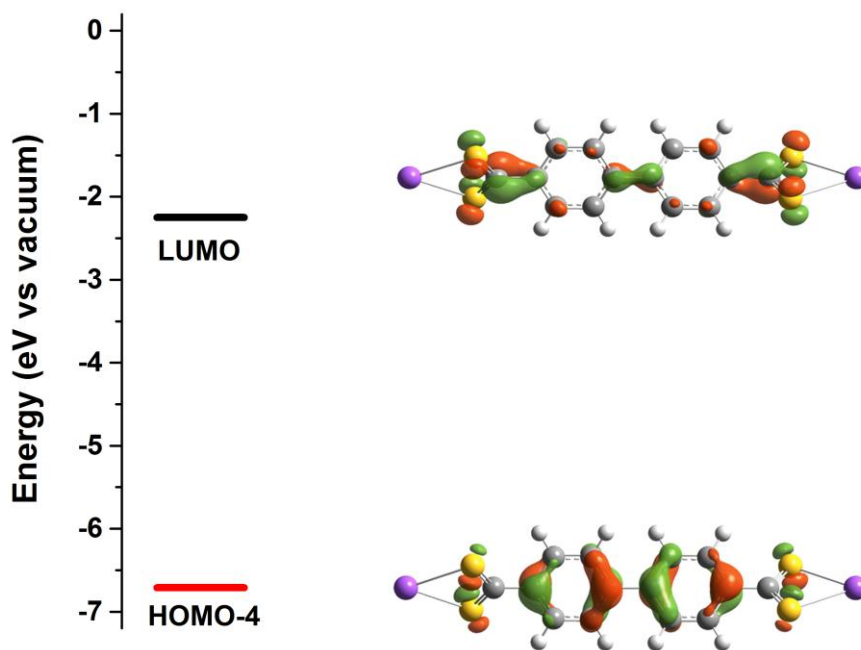


Figure S17. Computed frontier orbitals of **d** in DMF with an isocontour value of 0.05 at the TD-PBE0/6-311++G(d,p) level of theory in the PCM model.

S12. Cyclic voltammograms in DMF

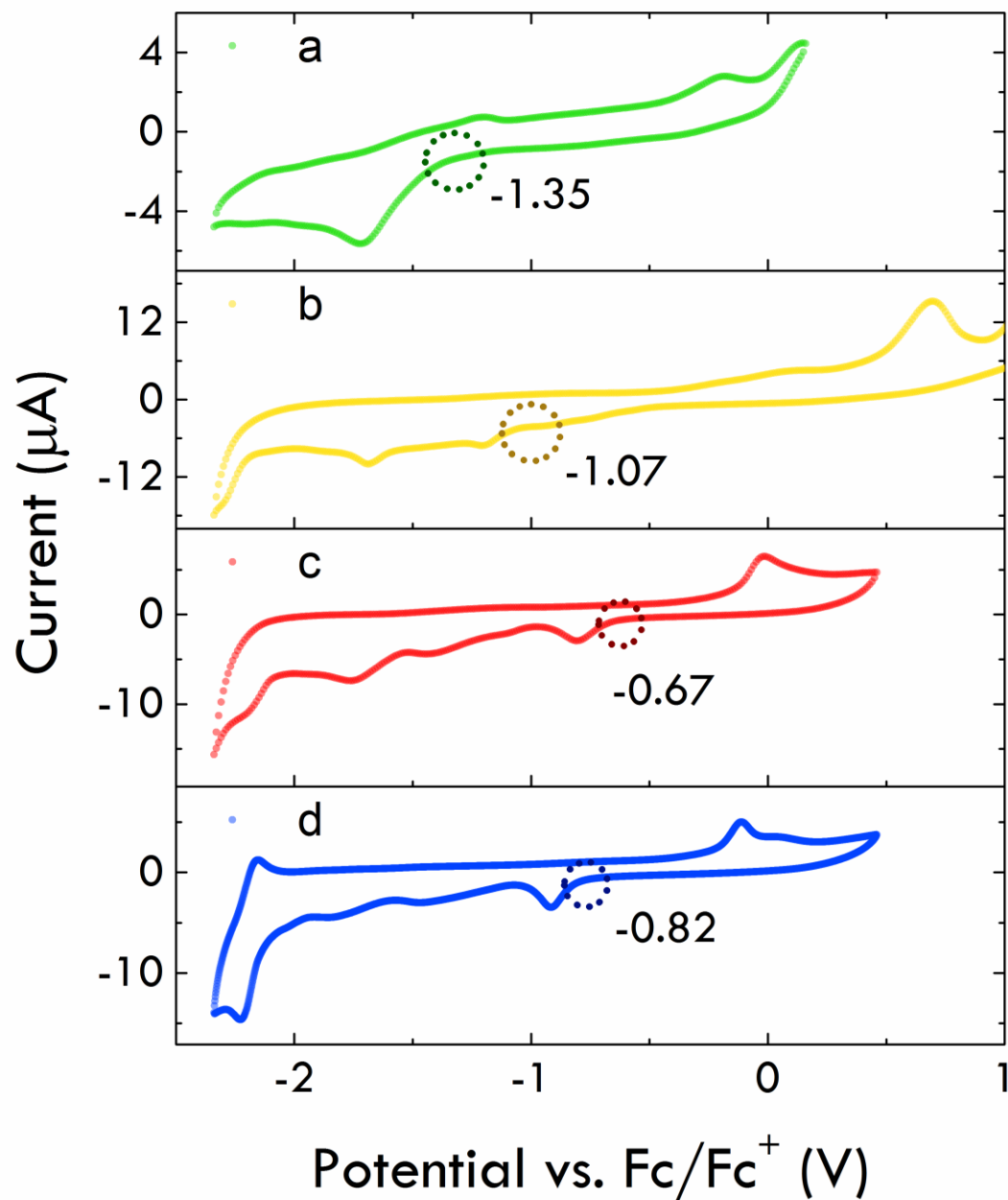
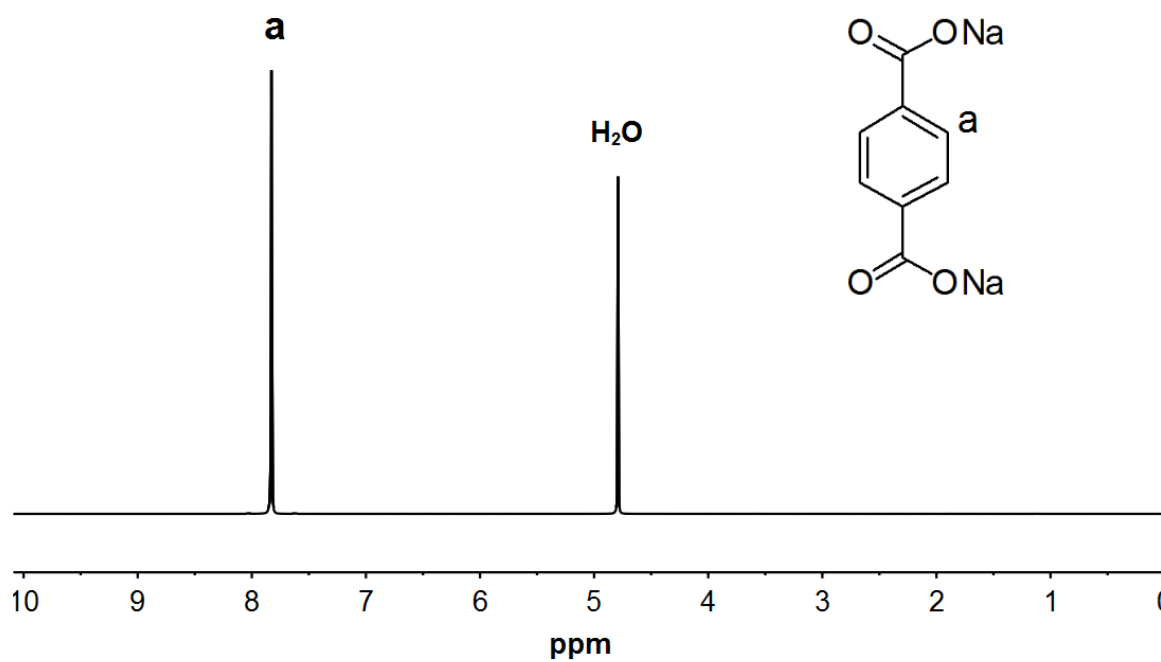
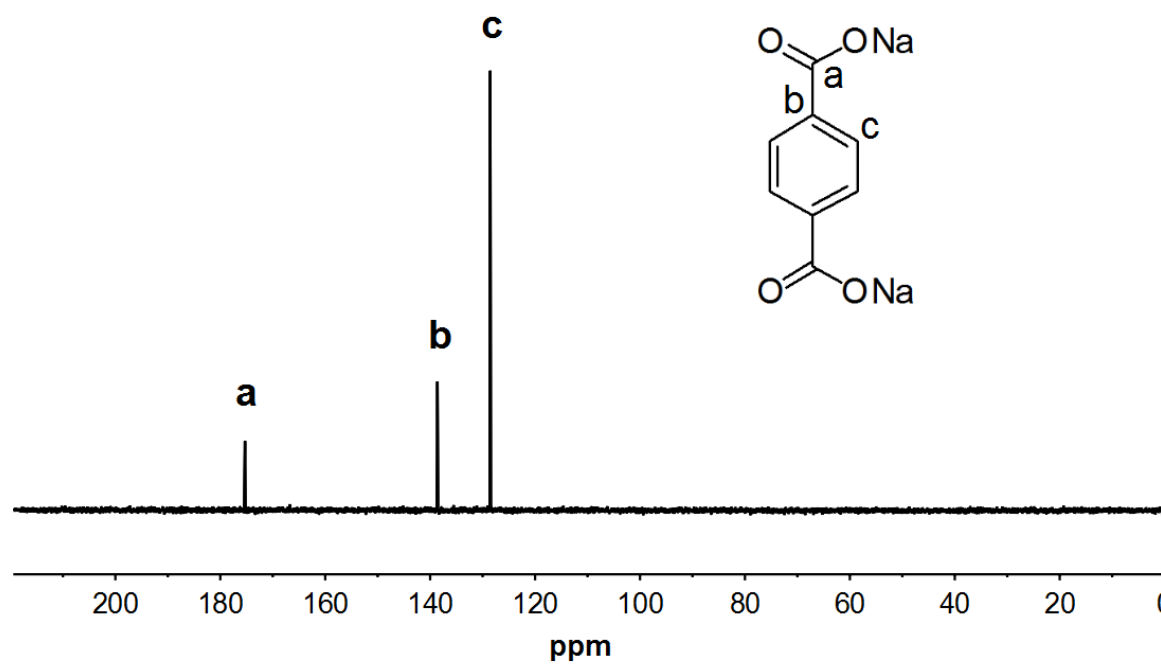


Figure S18. Cyclic voltammograms in DMF with Bu_4NPF_6 as a supporting electrolyte, Fc = ferrocene. Scan rate:

0.05 V/s. $T=25^\circ\text{C}$.

S13. NMR spectra of the sulfur-substituted dicarboxylate

Figure S19. ^1H NMR spectrum for sodium terephthalate in deuterated water.Figure S20. ^{13}C NMR spectrum for sodium terephthalate in deuterated water.

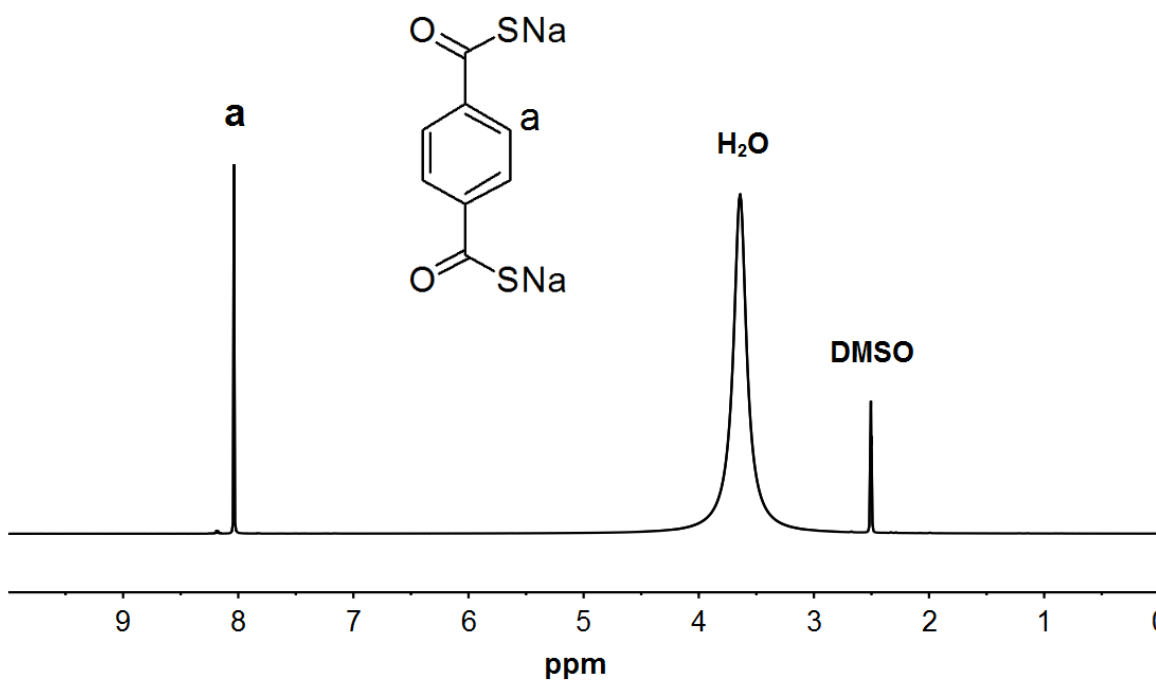


Figure S21. ^1H NMR spectrum for sodium 1,4-dithiophthalate.

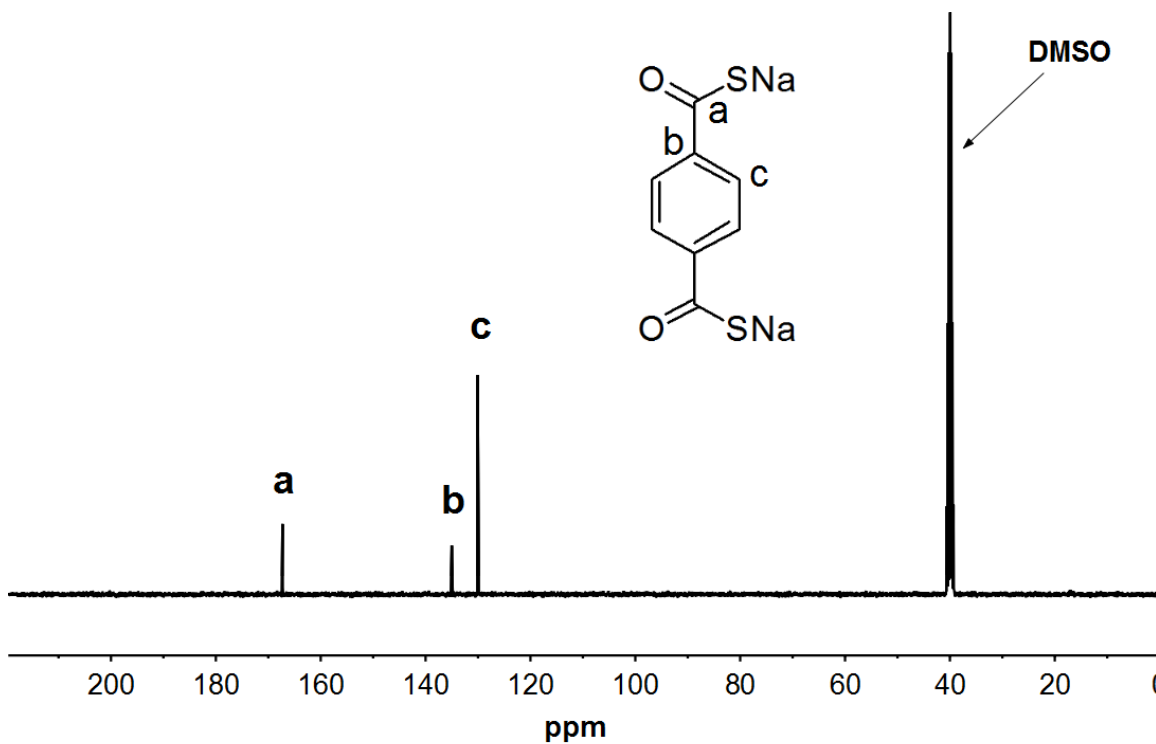


Figure S22. ^{13}C NMR spectrum for sodium 1,4-dithiophthalate.

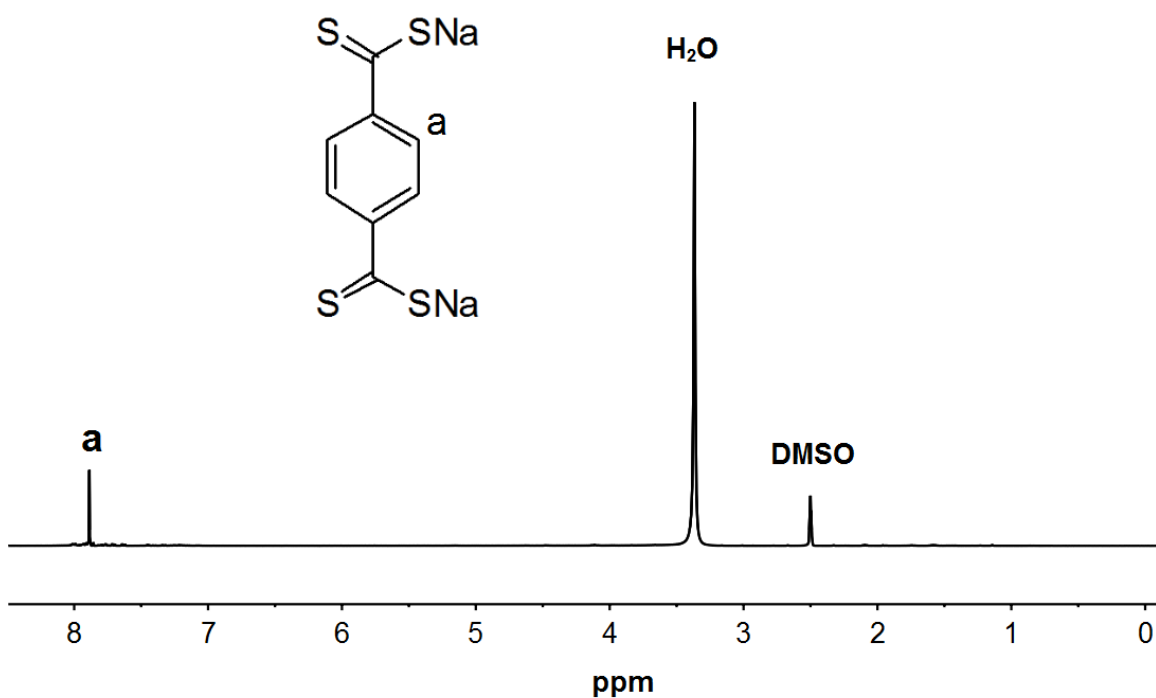


Figure S23. ¹H NMR spectrum for sodium tetrathioterephthalate.

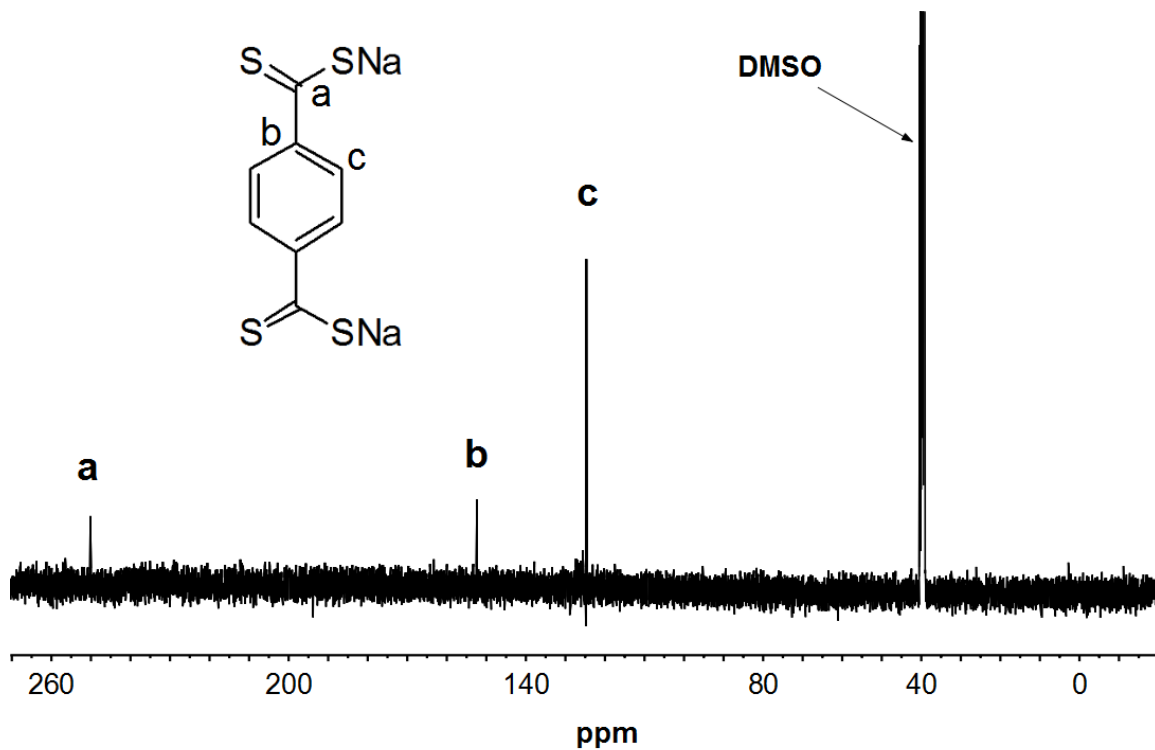


Figure S24. ¹³C NMR spectrum for sodium tetrathioterephthalate.

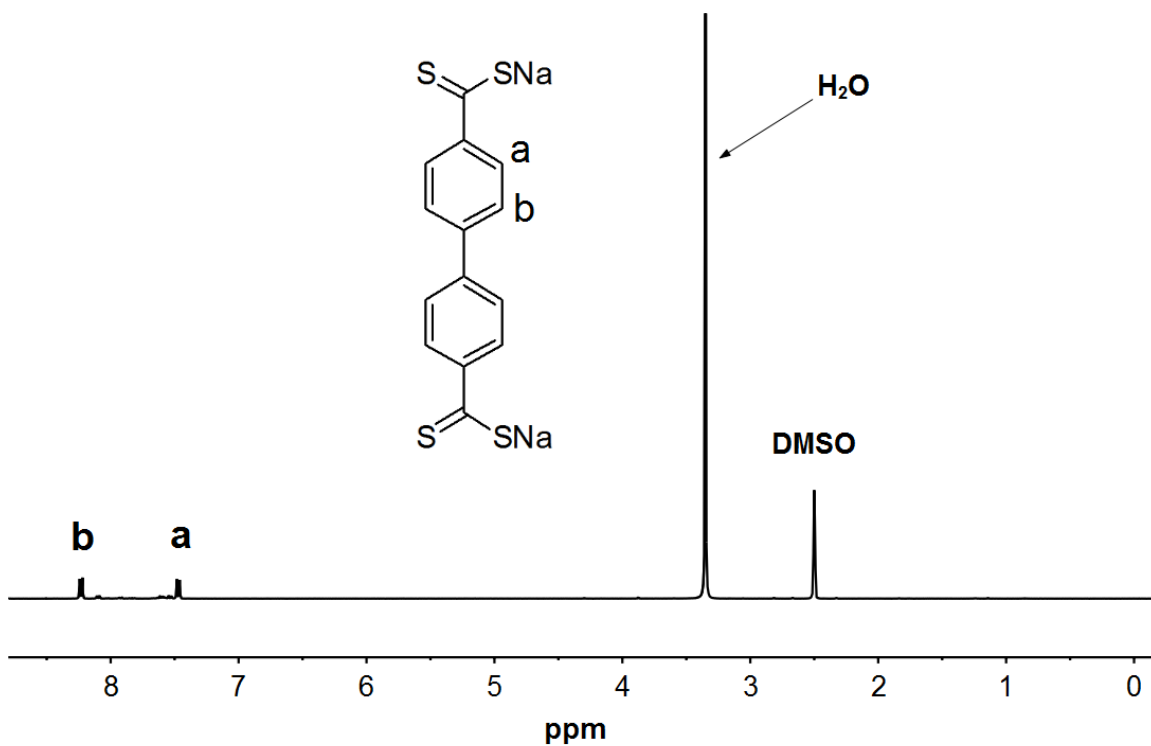


Figure S25. ¹H NMR spectrum for sodium 4,4'-biphenyltetrathiodicarboxylate.

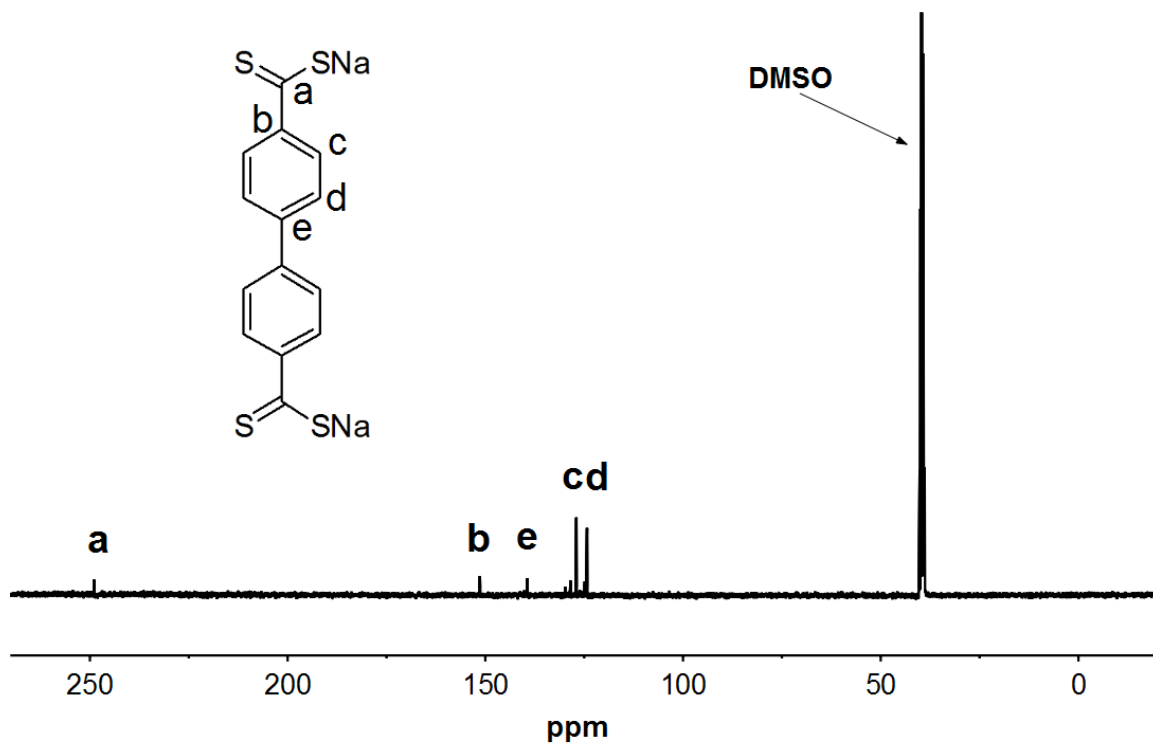


Figure S26. ¹³C NMR spectrum for sodium 4,4'-biphenyltetrathiodicarboxylate.

S14. Electrochemical results

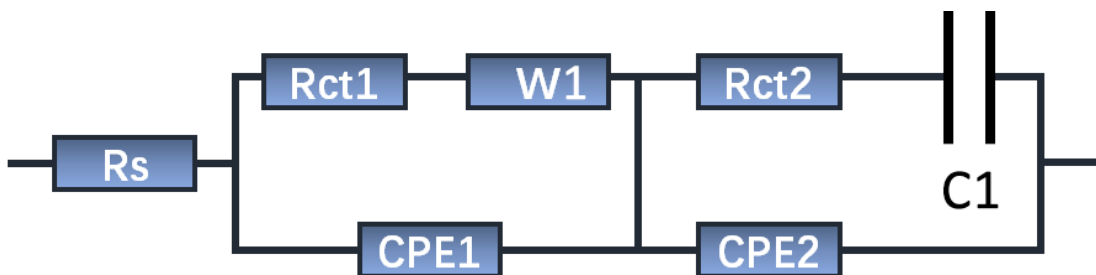


Figure S27. Equivalent circuit of molecule **a** and molecule **c** at 0V.

Table S2. EIS fitting results of compound **a** and compound **c**

	Rs	Rct 1	Rct 2	CPE 1	CPE 2	W1	C1
Compound a	3.67	150	27	1.5×10^{-5}	6×10^{-4}	0.018	0.14
Compound c	3.00	94	85	1×10^{-5}	5×10^{-3}	0.022	0.08

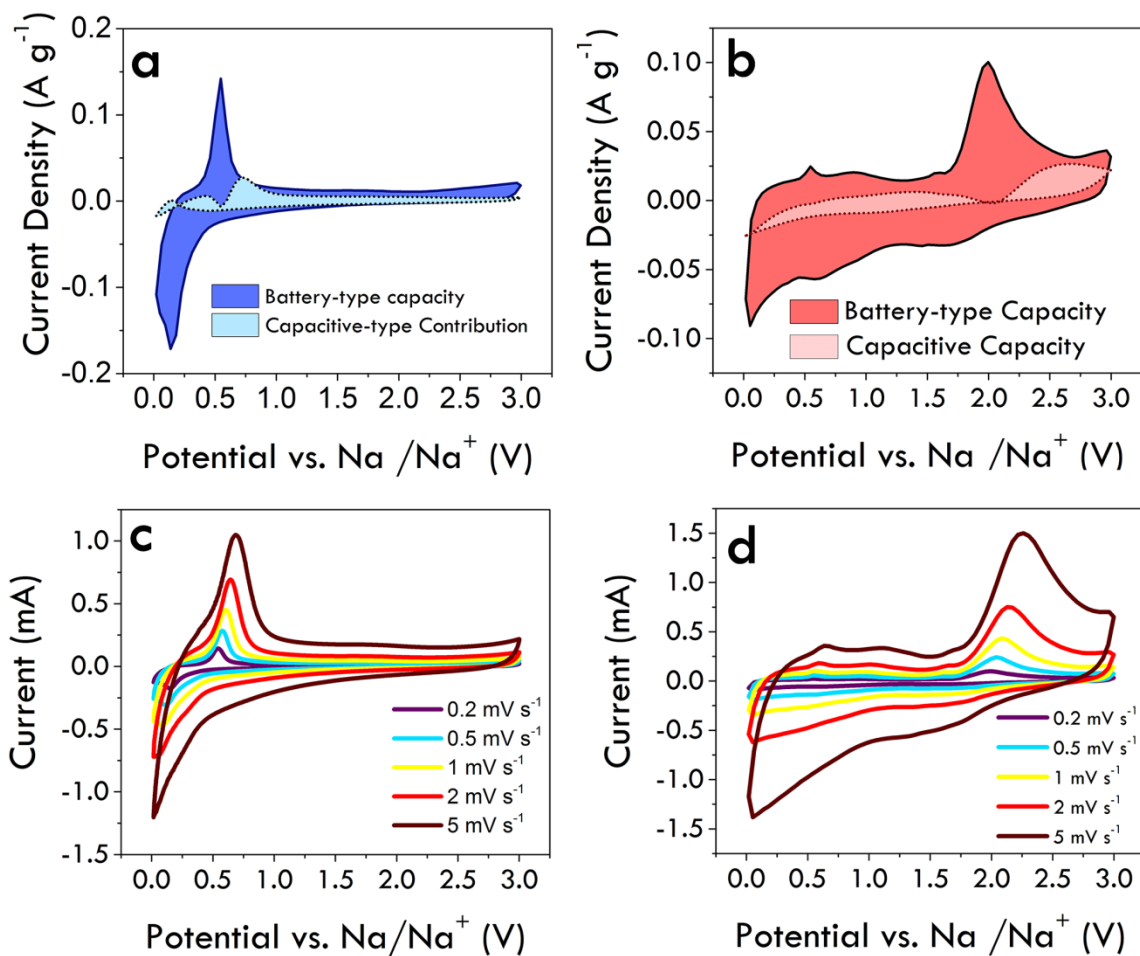


Figure S28. (1) battery-type and capacitive capacity contributions calculated from CV scans. a for compound a, b for compound c. (2) series cyclic voltammetry scans from 0.2-5 mV s⁻¹. c for compound a, d for compound c.

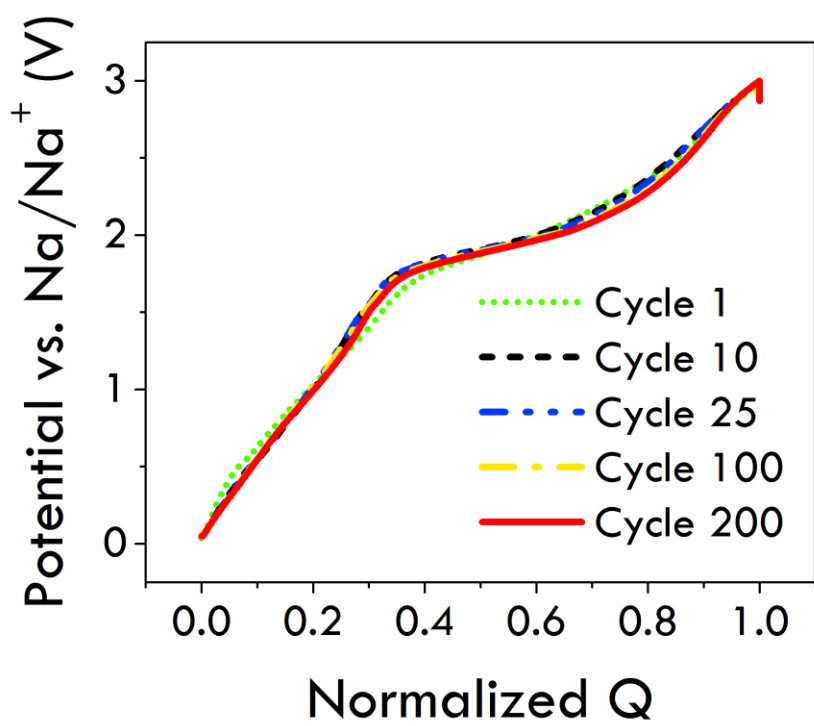


Figure S29. Normalized charge curves from 1 to 200 cycles for compound c.

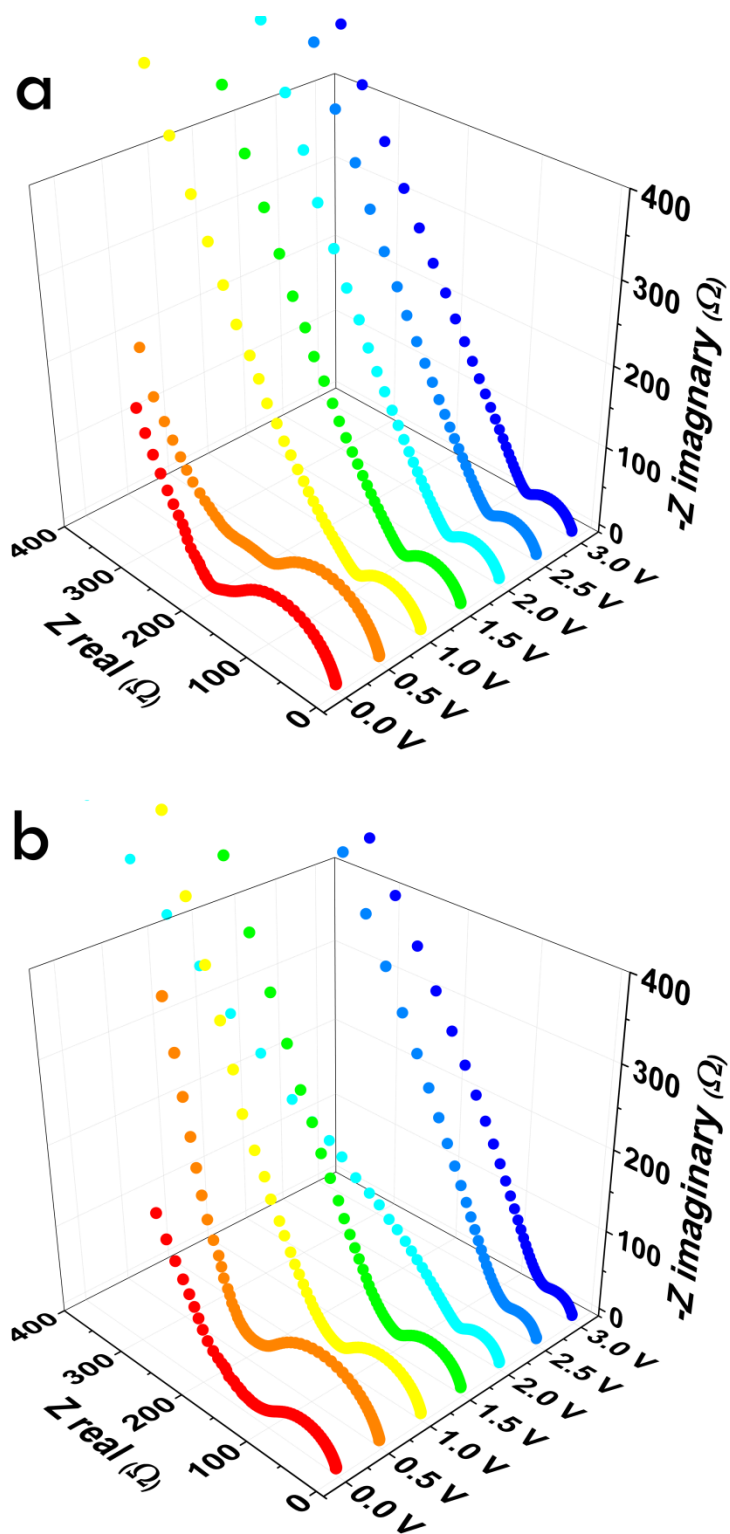


Figure S30. Electrochemical impedance spectroscopy at various potential. (a) EIS plots of molecule **a**. (b) EIS plots of molecule **c**.

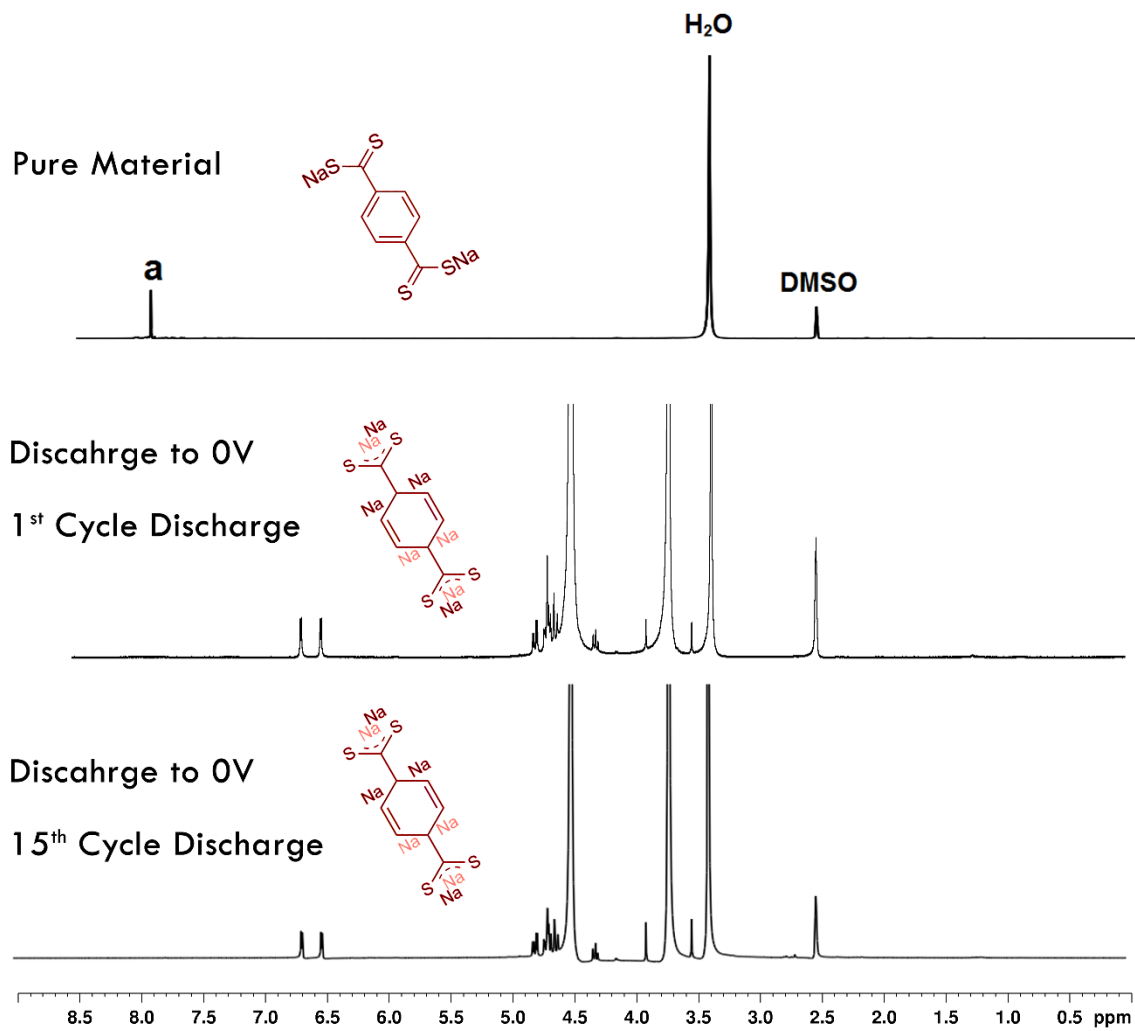


Figure S31. ^1H NMR spectrum for pristine sodium tetrathioterephthalate and after discharge to 0V.

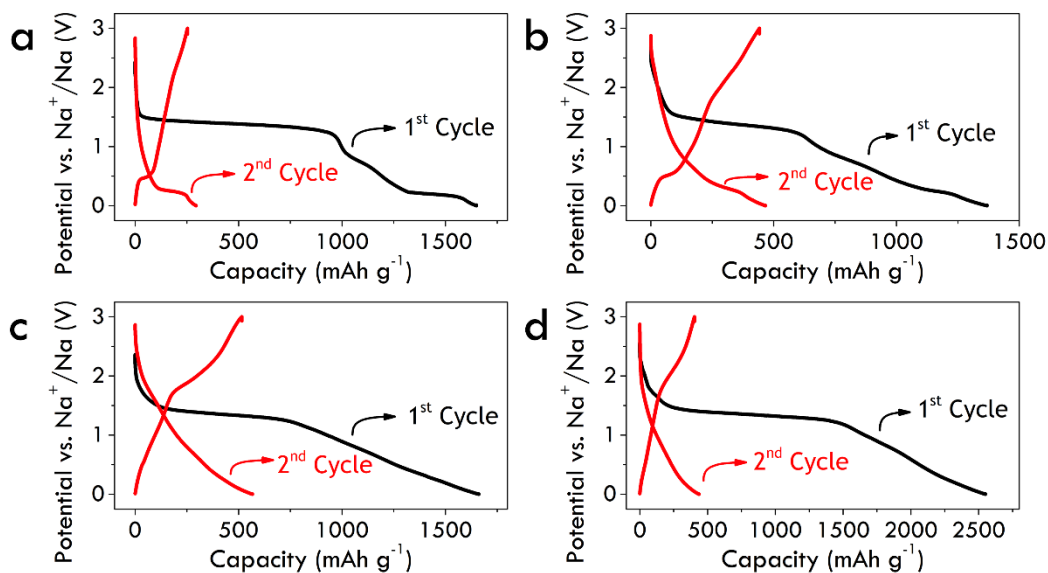


Figure S32. Initial charge/discharge curves of molecule (a) **a**, (b) **b**, (c) **c**, and (d) **d**.

Table S3. Theoretical capacities and utilization efficiencies of compound **a**, **b**, **c**, and **d**.

Compound	a	b	c	d
Theoretical Capacity (mAh g⁻¹)	255	443	586	459
Capacity at 50 mA g⁻¹ (mAh g⁻¹)	294	466	567	436
Utilization Efficiency* (%)	115%	105%	96%	95%

*The Utilization Efficiency exceeding 100% was possibly due to the contribution of carbon black.^[21]

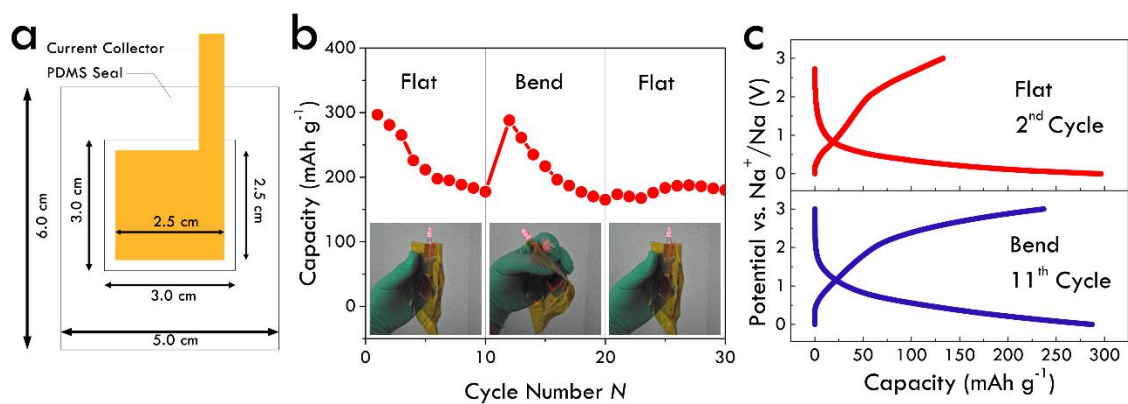


Figure S33. (a) The size of the flexible battery, (b) bending test of the battery, (c) charge-discharge curve of the battery in the flat and bend state.

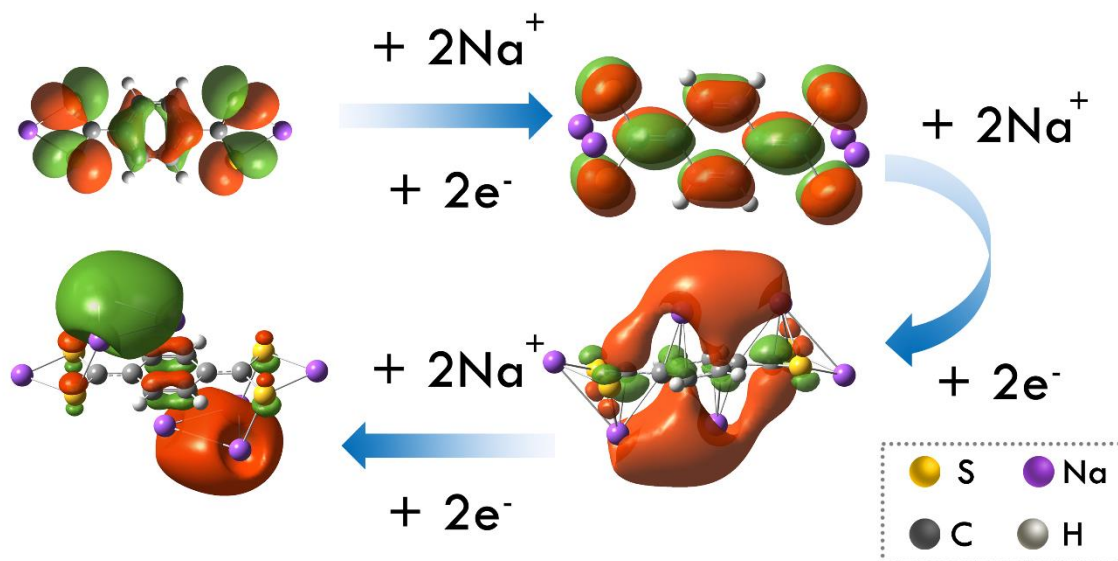


Figure S34. The HOMO orbitals with isocontour value of 0.03 during sodiation for molecule **c**.

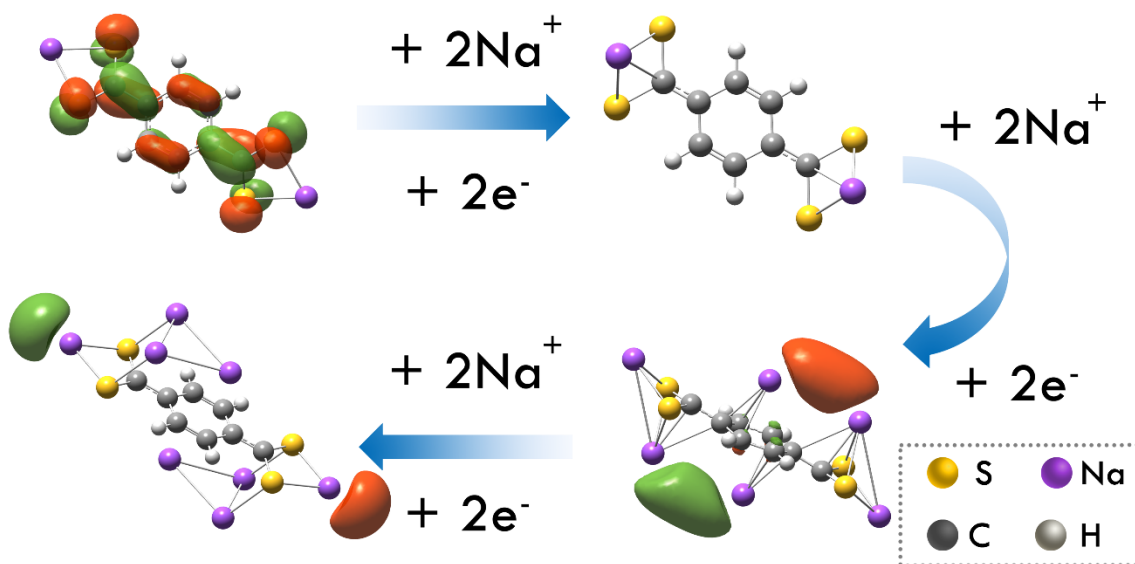
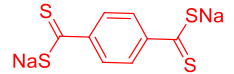
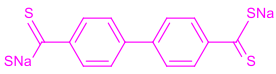
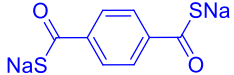
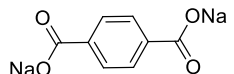
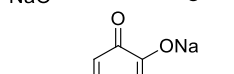
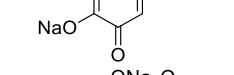
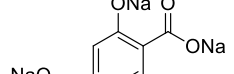
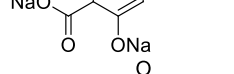
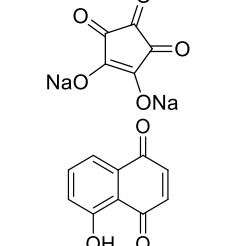
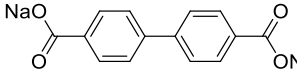
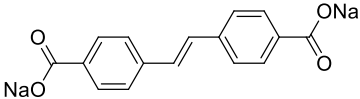
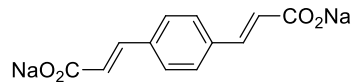
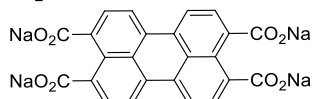
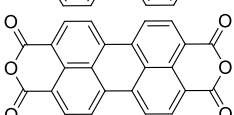
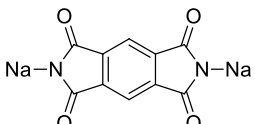
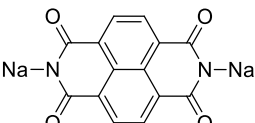


Figure S35. The LUMO orbitals with isocontour value of 0.02 during sodiation for molecule **c**.

S15. Comparison of the present sodium anode materials

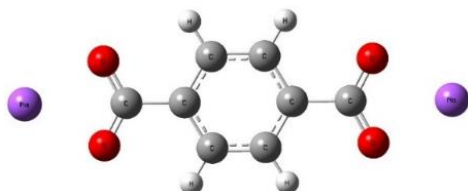
Table S4. Comparison of the present sodium anode materials

Structure	Electrode composition	Capacity (mAh g ⁻¹), current	Cycling stability: retention, cycles, current	Ref.
	60:30:10; c:Super P:CMC	567, 50 mA g⁻¹	65%, 100, 500 mA g ⁻¹	This work
	60:30:10; d:Super P:CMC	436, 50 mA g⁻¹	50%, 100, 500 mA g ⁻¹	This work
	60:30:10; b:Super P:CMC	466, 50 mA g⁻¹	48%, 100, 500 mA g ⁻¹	This work
	60:30:10; a:Super P:CMC	294, 50 mA g⁻¹	45%, 100, 500 mA g ⁻¹	This work
	50:37.5:12.5; 10 :Super P:CMC	295, 30 mA g ⁻¹	90%, 100, 40 mA g ⁻¹	10
	60:30:10; 11 :conductive carbon:PVdF	265, 0.1C	81%, 300, 1C	11
	65:30:5; 12 :Super P:PVdF	207, 0.1C	89%, 100, n.r.	12
	25.9:44.1:20:10; 13 :GOshell:CB:PVdF	293, 20 mA g ⁻¹	~40%, 100, 20 mA g ⁻¹	13
	30.4:69.6; 14 :reduced GO	398, 50 mA g ⁻¹	69.5%, 300, 100mA g ⁻¹	14

	57.1:28.6:14.3; 15 :Super P:CMC	200, 0.1C	~100%, 150, 0.1C	15
	50:40:10; 16 :CB:CMC	260, 50 mA g ⁻¹	70%, 400, 1 A g ⁻¹	16
	60:33:7; 17 :CB:CMC	177.7, 0.025C	~40 mA h g ⁻¹ , 40, 0.025C	17
	60:30:10; 18a :acetylene black:CMC	350.6, n.r.	37.4%, 120, 25 mA g ⁻¹	18a
	60:30:10; 18b :acetylene black:CMC	361, 25 mA g ⁻¹	40.4%, 140, 25 mA g ⁻¹	18b
	6:3:1; 19 :Super P:PVdF	128.9, 0.025C	70%, 100, 0.025C	19
	60:30:10; 20 :CB:PVdF	62, 6C	74%, 500, 6C	20

S16. Coordinates of molecular structures

All coordinates are reported as XYZ Cartesian coordinates. Converged geometries and the thermochemistry were also obtained from M06-2X/6-311++G(d,p) level of theory in PCM-described solvents (water or DMF). They are stated in Hartrees units. All energies reported were calculated using the GAUSSIAN 09 ver. B.01 computational chemistry package.

(a)**Gas phase**

Standard orientation:

Center Number	Atomic Number	Atomic Type	Coordinates (Angstroms)		
			X	Y	Z
1	6	0	0.000000	1.207114	0.694434
2	6	0	0.000000	0.000000	1.392380
3	6	0	0.000000	-1.207114	0.694434
4	6	0	0.000000	-1.207114	-0.694434
5	6	0	0.000000	0.000000	-1.392380
6	6	0	0.000000	1.207114	-0.694434
7	1	0	0.000000	2.130559	1.260381
8	1	0	0.000000	-2.130559	1.260381
9	1	0	0.000000	-2.130559	-1.260381
10	1	0	0.000000	2.130559	-1.260381
11	6	0	0.000000	0.000000	-2.899316
12	6	0	0.000000	0.000000	2.899316
13	8	0	0.000000	1.111368	-3.497820
14	8	0	0.000000	-1.111368	-3.497820
15	11	0	0.000000	0.000000	-5.374687
16	8	0	0.000000	-1.111368	3.497820
17	8	0	0.000000	1.111368	3.497820
18	11	0	0.000000	0.000000	5.374687

Zero-point correction= 0.109485

Thermal correction to Energy= 0.122166

Thermal correction to Enthalpy= 0.123111

Thermal correction to Gibbs Free Energy= 0.069640

Sum of electronic and zero-point Energies= -932.689822

Sum of electronic and thermal Energies= -932.677141

Sum of electronic and thermal Enthalpies= -932.676196

Sum of electronic and thermal Free Energies= -932.729667

Water solvent

Standard orientation:

Center Number	Atomic Number	Atomic Type	Coordinates (Angstroms)		
			X	Y	Z
1	6	0	-1.203412	0.695155	-0.018534
2	6	0	0.000000	1.401525	-0.017317
3	6	0	1.203412	0.695155	-0.018534
4	6	0	1.203412	-0.695155	-0.018534
5	6	0	0.000000	-1.401525	-0.017317
6	6	0	-1.203412	-0.695155	-0.018534
7	1	0	-2.133949	1.249430	-0.017888
8	1	0	2.133949	1.249430	-0.017888
9	1	0	2.133949	-1.249430	-0.017888
10	1	0	-2.133949	-1.249430	-0.017888
11	6	0	0.000000	-2.920739	-0.009557
12	6	0	0.000000	2.920739	-0.009557
13	8	0	-1.111533	-3.506727	-0.005226
14	8	0	1.111533	-3.506727	-0.005226
15	11	0	0.000000	-5.569380	0.045731
16	8	0	1.111533	3.506727	-0.005226
17	8	0	-1.111533	3.506727	-0.005226
18	11	0	0.000000	5.569380	0.045731

Zero-point correction= 0.107481

Thermal correction to Energy= 0.121055

Thermal correction to Enthalpy= 0.121999

Thermal correction to Gibbs Free Energy= 0.064559

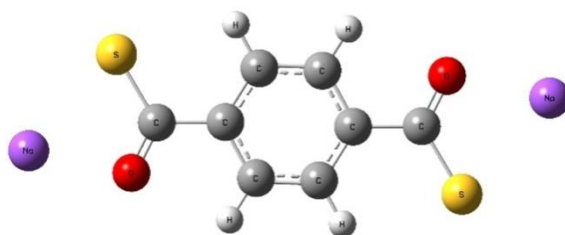
Sum of electronic and zero-point Energies= -932.788190

Sum of electronic and thermal Energies= -932.774616

Sum of electronic and thermal Enthalpies= -932.773672

Sum of electronic and thermal Free Energies= -932.831113

(b)



Gas phase

Standard orientation:

Center Number	Atomic Number	Atomic Type	Coordinates (Angstroms)		
			X	Y	Z
1	6	0	-0.009376	1.388268	0.000000
2	6	0	1.208782	0.703896	0.000000
3	6	0	1.208782	-0.692006	0.000000
4	6	0	0.009376	-1.388268	0.000000
5	6	0	-1.208782	-0.703896	0.000000
6	6	0	-1.208782	0.692006	0.000000
7	1	0	0.004048	2.470597	0.000000
8	1	0	2.153651	-1.220333	0.000000
9	1	0	-0.004048	-2.470597	0.000000
10	1	0	-2.153651	1.220333	0.000000
11	6	0	-2.478183	-1.511180	0.000000
12	6	0	2.478183	1.511180	0.000000
13	11	0	-4.499285	-3.244029	0.000000
14	11	0	4.499285	3.244029	0.000000
15	16	0	-4.012025	-0.704420	0.000000
16	16	0	4.012025	0.704420	0.000000
17	8	0	2.370167	2.752729	0.000000
18	8	0	-2.370167	-2.752729	0.000000

Zero-point correction= 0.104258

Thermal correction to Energy= 0.118017

Thermal correction to Enthalpy= 0.118962

Thermal correction to Gibbs Free Energy= 0.060719

Sum of electronic and zero-point Energies= -1578.600405

Sum of electronic and thermal Energies= -1578.586646

Sum of electronic and thermal Enthalpies= -1578.585702

Sum of electronic and thermal Free Energies= -1578.643944

DMF solvent

Standard orientation:

Center Number	Atomic Number	Atomic Type	Coordinates (Angstroms)		
			X	Y	Z
1	6	0	0.684475	1.205978	0.018191
2	6	0	1.404597	0.007997	-0.001360
3	6	0	0.703854	-1.199627	-0.019653
4	6	0	-0.684475	-1.205978	-0.018191
5	6	0	-1.404597	-0.007997	0.001360
6	6	0	-0.703854	1.199627	0.019653
7	1	0	1.228245	2.141898	0.032684
8	1	0	1.254693	-2.131369	-0.035134
9	1	0	-1.228245	-2.141898	-0.032684
10	1	0	-1.254693	2.131369	0.035134
11	6	0	-2.915917	-0.080196	0.002666
12	6	0	2.915917	0.080196	-0.002666
13	11	0	-5.708645	-0.813053	-0.002017
14	11	0	5.708645	0.813053	-0.002017
15	16	0	-3.855869	1.373948	-0.000826
16	16	0	3.855869	-1.373948	0.000826
17	8	0	3.431331	1.205546	-0.005219
18	8	0	-3.431331	-1.205546	0.005219

Zero-point correction= 0.102921

Thermal correction to Energy= 0.117263

Thermal correction to Enthalpy= 0.118207

Thermal correction to Gibbs Free Energy= 0.057275

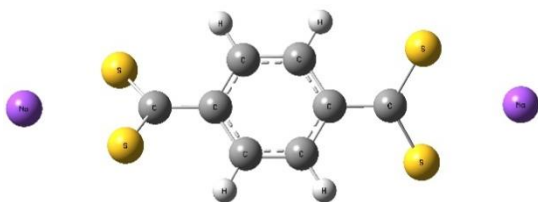
Sum of electronic and zero-point Energies= -1578.692398

Sum of electronic and thermal Energies= -1578.678057

Sum of electronic and thermal Enthalpies= -1578.677112

Sum of electronic and thermal Free Energies= -1578.738044

(c)



Gas phase

Standard orientation:

Center Number	Atomic Number	Atomic Type	Coordinates (Angstroms)		
			X	Y	Z
1	6	0	-0.012989	1.201821	0.692299
2	6	0	0.000000	0.000000	1.409413
3	6	0	0.012989	-1.201821	0.692299
4	6	0	-0.012989	-1.201821	-0.692299
5	6	0	0.000000	0.000000	-1.409413
6	6	0	0.012989	1.201821	-0.692299
7	1	0	-0.030333	2.139372	1.232385
8	1	0	0.030333	-2.139372	1.232385
9	1	0	-0.030333	-2.139372	-1.232385
10	1	0	0.030333	2.139372	-1.232385
11	6	0	0.000000	0.000000	-2.903138
12	6	0	0.000000	0.000000	2.903138
13	11	0	0.000000	0.000000	-5.812735
14	11	0	0.000000	0.000000	5.812735
15	16	0	-0.749955	-1.310047	-3.687938
16	16	0	0.749955	1.310047	-3.687938
17	16	0	0.749955	-1.310047	3.687938
18	16	0	-0.749955	1.310047	3.687938

Zero-point correction= 0.099248

Thermal correction to Energy= 0.113930

Thermal correction to Enthalpy= 0.114874

Thermal correction to Gibbs Free Energy= 0.054860

Sum of electronic and zero-point Energies= -2224.506289

Sum of electronic and thermal Energies= -2224.491608

Sum of electronic and thermal Enthalpies= -2224.490663

Sum of electronic and thermal Free Energies= -2224.550677

DMF solvent

Standard orientation:

Center Number	Atomic Number	Atomic Type	Coordinates (Angstroms)		
			X	Y	Z
1	6	0	-0.014735	1.201255	0.693237
2	6	0	0.000000	0.000000	1.411354
3	6	0	0.014735	-1.201255	0.693237
4	6	0	-0.014735	-1.201255	-0.693237
5	6	0	0.000000	0.000000	-1.411354
6	6	0	0.014735	1.201255	-0.693237
7	1	0	-0.033164	2.139821	1.232715
8	1	0	0.033164	-2.139821	1.232715
9	1	0	1.232715	-2.139821	-1.232715
10	1	0	0.033164	2.139821	-1.232715
11	6	0	0.000000	0.000000	-2.907516
12	6	0	0.000000	0.000000	2.907516
13	11	0	0.000000	0.000000	-6.137382
14	11	0	0.000000	0.000000	6.137382
15	16	0	-0.885139	-1.204550	-3.704352
16	16	0	0.885139	1.204550	-3.704352
17	16	0	0.885139	-1.204550	3.704352
18	16	0	-0.885139	1.204550	3.704352

Zero-point correction= 0.097633

Thermal correction to Energy= 0.113193

Thermal correction to Enthalpy= 0.114137

Thermal correction to Gibbs Free Energy= 0.050827

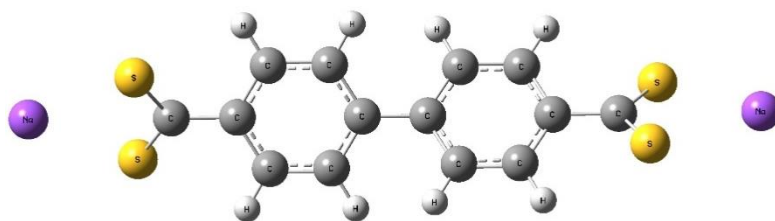
Sum of electronic and zero-point Energies= -2224.597201

Sum of electronic and thermal Energies= -2224.581641

Sum of electronic and thermal Enthalpies= -2224.580696

Sum of electronic and thermal Free Energies= -2224.644007

(d)

**Gas phase**

Standard orientation:

Center Number	Atomic Number	Atomic Type	Coordinates (Angstroms)		
			X	Y	Z
1	6	0	-0.392195	1.133801	-1.458791
2	6	0	0.000000	0.000000	-0.740042
3	6	0	0.392195	-1.133801	-1.458791
4	6	0	0.403457	-1.131274	-2.844417
5	6	0	0.000000	0.000000	-3.564198
6	6	0	-0.403457	1.131274	-2.844417
7	1	0	-0.720422	2.018122	-0.924555
8	1	0	0.720422	-2.018122	-0.924555
9	1	0	0.728054	-2.011417	-3.383874
10	1	0	-0.728054	2.011417	-3.383874
11	6	0	0.000000	0.000000	-5.058074
12	11	0	0.000000	0.000000	-7.976437
13	16	0	1.035808	-1.094534	-5.850213
14	16	0	-1.035808	1.094534	-5.850213
15	6	0	0.000000	0.000000	0.740042
16	6	0	-0.392195	-1.133801	1.458791
17	6	0	0.392195	1.133801	1.458791
18	6	0	-0.403457	-1.131274	2.844417
19	1	0	-0.720422	-2.018122	0.924555
20	6	0	0.403457	1.131274	2.844417
21	1	0	0.720422	2.018122	0.924555
22	6	0	0.000000	0.000000	3.564198
23	1	0	-0.728054	-2.011417	3.383874
24	1	0	0.728054	2.011417	3.383874
25	6	0	0.000000	0.000000	5.058074
26	16	0	1.035808	1.094534	5.850213

27	16	0	-1.035808	-1.094534	5.850213
28	11	0	0.000000	0.000000	7.976437

Zero-point correction= 0.180574

Thermal correction to Energy= 0.199946

Thermal correction to Enthalpy= 0.200890

Thermal correction to Gibbs Free Energy= 0.128795

Sum of electronic and zero-point Energies= -2455.443373

Sum of electronic and thermal Energies= -2455.424001

Sum of electronic and thermal Enthalpies= -2455.423057

Sum of electronic and thermal Free Energies= -2455.495152

DMF solvent

Standard orientation:

Center Number	Atomic Number	Atomic Type	Coordinates (Angstroms)		
			X	Y	Z
1	6	0	-1.130212	1.465004	-0.442386
2	6	0	0.002688	0.740871	-0.054809
3	6	0	1.139872	1.453417	0.341756
4	6	0	1.136720	2.840359	0.372672
5	6	0	0.007340	3.563915	-0.026489
6	6	0	-1.122398	2.852598	-0.445690
7	1	0	-2.019861	0.937638	-0.767805
8	1	0	2.027208	0.916763	0.658088
9	1	0	2.017244	3.375539	0.705439
10	1	0	-2.001383	3.397489	-0.766761
11	6	0	0.006540	5.058804	0.000494
12	11	0	0.002688	8.286434	0.104044
13	16	0	0.814249	5.829013	1.275832
14	16	0	-0.801461	5.880697	-1.241253
15	6	0	-0.002688	-0.740871	-0.054809
16	6	0	1.130212	-1.465004	-0.442386
17	6	0	-1.139872	-1.453417	0.341756
18	6	0	1.122398	-2.852598	-0.445690
19	1	0	2.019861	-0.937638	-0.767805
20	6	0	-1.136720	-2.840359	0.372672
21	1	0	-2.027208	-0.916763	0.658088

22	6	0	-0.007340	-3.563915	-0.026489
23	1	0	2.001383	-3.397489	-0.766761
24	1	0	-2.017244	-3.375539	0.705439
25	6	0	-0.006540	-5.058804	0.000494
26	16	0	-0.814249	-5.829013	1.275832
27	16	0	0.801461	-5.880697	-1.241253
28	11	0	-0.002688	-8.286434	0.104044

Zero-point correction= 0.179535

Thermal correction to Energy= 0.199296

Thermal correction to Enthalpy= 0.200240

Thermal correction to Gibbs Free Energy= 0.128331

Sum of electronic and zero-point Energies= -2455.535206

Sum of electronic and thermal Energies= -2455.515445

Sum of electronic and thermal Enthalpies= -2455.514501

Sum of electronic and thermal Free Energies= -2455.586410

S17. References

- (1) M. J. Frisch, G. W. Trucks, H. B. Schlegel, G. E. Scuseria, M. A. Robb, J. R. Cheeseman, G. Scalmani, V. Barone, B. Mennucci, G. A. Petersson, H. Nakatsuji, M. Caricato, X. Li, H. P. Hratchian, A. F. Izmaylov, J. Bloino, G. Zheng, J. L. Sonnenberg, M. Hada, M. Ehara, K. Toyota, R. Fukuda, J. Hasegawa, M. Ishida, T. Nakajima, Y. Honda, O. Kitao, H. Nakai, T. Vreven, Jr., J. A. Montgomery, J. E. Peralta, F. Ogliaro, M. Bearpark, J. J. Heyd, E. Brothers, K. N. Kudin, V. N. Staroverov, R. Kobayashi, J. Normand, K. Raghavachari, A. Rendell, J. C. Burant, S. S. Iyengar, J. Tomasi, M. Cossi, N. Rega, J. M. Millam, M. Klene, J. E. Knox, J. B. Cross, V. Bakken, C. Adamo, J. Jaramillo, R. Gomperts, R. E. Stratmann, O. Yazyev, A. J. Austin, R. Cammi, C. Pomelli, J. W. Ochterski, R. L. Martin, K. Morokuma, V. G. Zakrzewski, G. A. Voth, P. Salvador, J. J. Dannenberg, S. Dapprich, A. D. Daniels, Ö. Farkas, J. B. Foresman, J. V. Ortiz, J. Cioslowski, D. J. Fox, Gaussian 09, Revision B.01; Gaussian, Inc., Wallingford, CT, **2010**.
- (2) J. Tomasi, B. Mennucci, R. Cammi, *Chem. Rev.* **2005**, *105*, 2999-3093.
- (3) R.G. Parr, W. Yang, *Oxford University Press*, New York, **1989**.
- (4) W. Koch, M. C. Holthausen, Wiley-VCH, Weinheim, **2000**.
- (5) Y. Zhao, D. G. Truhlar, *Theor. Chem. Acc.* **2008**, *120*, 215-241.
- (6) Y. Zhao, D. G. Truhlar, *Acc. Chem. Res.* **2008**, *41*, 157-167.
- (7) R. Bauernschmitt, R. Ahlrichs, *Chem. Phys. Lett.* **1996**, *256*, 454-464.
- (8) M. E. Casida, C. Jamorski, K. C. Casida, D. R. Salahub, *J. Chem. Phys.* **1998**, *108*, 4439-4449.
- (9) C. Adamo, V. Barone, *J. Chem. Phys.* **1999**, *110*, 6158-6170.
- (10) Y. Park, D. S. Shin, S. H. Woo, N. S. Choi, K. H. Shin, S. M. Oh, K. T. Lee, S. Y. Hong, *Adv. Mater.* **2012**, *24*, 3562-3567.
- (11) Z. Zhu, H. Li, J. Liang, Z. Tao, J. Chen, *Chem. Commun.* **2015**, *51*, 1446-1448.
- (12) S. Wang, L. Wang, Z. Zhu, Z. Hu, Q. Zhao, J. Chen, *Angew. Chem. Int. Ed.* **2014**, *53*, 5892-5896.
- (13) C. Luo, Y. Zhu, Y. Xu, Y. Liu, T. Gao, J. Wang, C. Wang, *J. Power Sources* **2014**, *250*, 372-378.
- (14) H. Wang, P. Hu, J. Yang, G. Gong, L. Guo, X. Chen, *Adv. Mater.* **2015**, *27*, 2348-2354.
- (15) A. Choi, Y. K. Kim, T. K. Kim, M. S. Kwon, K. T. Lee, H. R. Moon, *J. Mater. Chem. A* **2014**, *2*, 14986-14993.
- (16) C. Wang, Y. Xu, Y. Fang, M. Zhou, L. Liang, S. Singh, H. Zhao, A. Schober, Y. Lei, *J. Am. Chem. Soc.* **2015**, *137*, 3124-3130.
- (17) V. A. Mihali, S. Renault, L. Nyholm, D. Brandell, *RSC Adv.* **2014**, *4*, 38004-38011.
- (18) H. G. Wang, S. Yuan, Z. Si, X. B. Zhang, *Energy Environ. Sci.* **2015**, *8*, 3160-3165.
- (19) S. Renault, V. A. Mihali, K. Edström, D. Brandell, *Electrochem. Commun.* **2014**, *45*, 52-55.
- (20) D. J. Kim, Y. H. Jung, K. K. Bharathi, S. H. Je, D. K. Kim, A. Coskun, J. W. Choi, *Adv. Energy Mater.* **2014**, *4*, 1400133.
- (21) C. Wang, Y. Xu, Y. Fang, M. Zhou, L. Liang, S. Singh, H. Zhao, A. Schober, Y. Lei, *J. Am. Chem. Soc.* **2015**, *137*, 3124-3130.

Author Contributions

Hongyang Zhao, Jianwei Wang, Gang He and Yaping Du conceived the idea for the study. Jianwei Wang prepared the samples and conducted characterizations. Hongyang Zhao conducted electrochemical measurements. Hongyang Zhao, Yuheng Zheng and Xiaogang Han analyzed the electrochemical data. Gang He and Ju Li contributed to the DFT calculations. Hongyang Zhao and Jianwei Wang, Gang He and Yaping Du wrote the manuscript and all the authors revised and polished the manuscript.